National Defence / Défense nationale

UNCLASSIFIED
UNLIMITED DISTRIBUTION

AD-A274 195

DREV REPORT 4712/93
DECEMBER 1993

CRDV RAPPORT 4712 93
DÉCEMBRE 1993

ANALYTIC APPROXIMATION TO RANDOMLY ORIENTED SPHEROID EXTINCTION

B.T.N. Evans and G.R. Fournier

RESEARCH AND DEVELOPMENT BRANCH
DEPARTMENT OF NATIONAL DEFENCE
CANADA

BUREAU - RECHERCHE ET DÉVELOPPEMENT
MINISTÈRE DE LA DÉFENSE NATIONALE
CANADA

Defence Research Establishment
Centre de recherches pour la Défense,
Valcartier, Québec

Canada

SANS CLASSIFICATION
DISTRIBUTION ILLIMITÉE

ANALYTIC APPROXIMATION TO RANDOMLY ORIENTED SPHEROID EXTINCTION

by

B.T.N. Evans and G.R. Fournier

DEFENCE RESEARCH ESTABLISHMENT
CENTRE DE RECHERCHES POUR LA DÉFENSE
VALCARTIER
Tel: (418) 844-4229

Québec, Canada December/décembre 1993

SANS CLASSIFICATION

ABSTRACT

An analytic semi-empirical approximation to the extinction efficiency, Q_{ext}, for randomly oriented spheroids, based on an extension of the anomalous diffraction formula, is given and compared with the extended boundary condition or T-matrix method. This will allow for better and more general modelling of obscurants. Using this formula, Q_{ext} can be evaluated over 10^4 times faster than with previous methods. This approximation has been verified for complex refractive indices $m = n - ik$, where $1 \leq n \leq \infty$ and $0 \leq k \leq \infty$ and aspect ratios from 0.2 to 5. We believe that the approximation is uniformly valid over all size parameters and aspect ratios. It has the correct Rayleigh, refractive index and large particle asymptotic behaviours. The accuracy and limitations of this formula are extensively discussed.

RÉSUMÉ

Nous présentons une approximation analytique semi-empirique de l'efficacité d'extinction Q_{ext}, pour des particules sphéroïdales orientées aléatoirement, basée sur une extension de la théorie de la diffraction anomalique. Cette approximation est comparée au calcul basé sur la méthode de conditions frontières étendues ou matrices de transition. Cette approximation permet de mieux modéliser les obscurants. Grâce à cette formule, Q_{ext} peut être évalué 10^4 fois plus vite que par les méthodes antérieures. Nous avons vérifié cette formule pour des indices de réfraction complexes $m = n - ik$, où $1 \leq n \leq \infty$ et $0 \leq k \leq \infty$ et pour des aspects de 0.2 à 5. Nous croyons que l'approximation est uniformément valide pour toutes les grosseurs et tous les aspects. Elle se comporte correctement à la limite de Rayleigh, à la limite de l'indice de réfraction infini et à la limite géométrique. L'exactitude de cette formule ainsi que ses limites sont discutées en détail.

TABLE OF CONTENTS

ABSTRACT/RÉSUMÉ i

EXECUTIVE SUMMARY v

1.0 INTRODUCTION 1

2.0 DEVELOPMENT OF THE EXTINCTION FORMULA 2

2.1 Small Particle Term 3
2.2 Large Particle Term 5
2.3 Bridging Function 13

3.0 RESULTS 16

4.0 CONCLUSIONS AND LIMITATIONS 25

5.0 ACKNOWLEDGEMENT 26

6.0 REFERENCES 27

FIGURES 1 to 11

APPENDIX A– Survey of Maximum Relative Error and its Location 29

EXECUTIVE SUMMARY

The present and future electro-optic capabilities of fire control systems require full spectrum obscurants as an effective countermeasure. It is well known that spherical particles can obscure efficiently only in the visible region of the spectrum. In the near and far infrared as well as in the microwave region of the spectrum the use of non-spherical particles is mandatory. Imaging through ocean waters and dusty environments both require knowledge of the extinction by non-spherical particles. Communications, remote sensing, surveillance and radar propagation frequently encounter scenarios involving non-spherical particles. The estimation of electromagnetic extinction through dust or other non-spherical atmospheric aerosols and hydrosols is an essential first step in the evaluation of the performance of all electro-optic systems.

To date, the theoretical exploration of the effect of these types of particles on the performance of obscurants has been either extremely restrictive or prohibitively expensive. This work partially overcomes these severe restrictions and will aid in the design and performance analysis of potential new obscurants. For instance, a factor greater than ten thousand in computational speed has been achieved with minimal loss in accuracy. Furthermore, the present approach is much more flexible in the sense that extremely elongated or flattened particles can now be modelled. Elongated particles are thought to be good millimeter wave obscurants and flattened or flake-like particles are known to be good infrared obscurants.

The immediate objective of this work is to significantly reduce the computational burden in calculating the extinction from non-spherical particles. This allows for the exploration of the effects of non-spherical particles.

The longer term goal of this work is to alleviate the remaining constraints in the theoretical consideration of non-spherical aerosols and obscurants of either natural or artificial origin. This will aid not only in finding better obscurants but also in the possible identification and remote classification of such aerosols.

1.0 INTRODUCTION

The immediate objective of this work is to significantly reduce the computational burden in calculating the extinction from non-spherical particles. This allows for the exploration of the effects of non-spherical particles on the performance of obscurants and electro-optical systems. The longer term goal of this work is to alleviate the remaining constraints in the theoretical consideration of non-spherical aerosols and obscurants of either natural or artificial origin. This will aid not only in finding better obscurants but also in the possible identification and remote classification of such aerosols.

We have previously presented (Ref. 1) a numerical approximation to Q_{ext} for randomly oriented spheroids. This work was applicable to particles with $1.01 \leq n \leq 2$ and $0 \leq k \leq 1$ for arbitrary sizes and aspect ratios. The required angular integration was carried out by a 64-point Gaussian quadrature. Since many materials have optical properties beyond the above limits, we have, in this work, extended the refractive index range to $1 \leq n \leq \infty$ and $0 \leq k \leq \infty$. Furthermore, large optical sizes produce high frequency oscillations in the kernel of the angular integral. These integrals are very difficult and time-consuming to estimate numerically. We have replaced this numerical integral with an approximate analytic expression that overcomes this difficulty.

The basic approach is to orthogonalize as much as possible the scattering physics into well-defined regimes. For small physical and optical sizes, the electrostatics (Rayleigh) approximation is used. For larger and very large optical sizes we still use the electrostatics

approximation but with the optical constants transformed (Ref. 2) to include the effects of the magnetic dipole. In the large physical size regime we split the physics into a diffraction (anomalous diffraction) component and what can be loosely described as edge effects. The diffraction component is modelled by the anomalous diffraction approximation as developed by Van de Hulst (Ref. 3). The edge effect (Fock theory) component is modelled by extending a technique introduced by Jones (Refs. 1 and 4). In this report, this component is further generalized to have proper behaviour at small optical sizes and for large indices. The gap between the large and small particle regimes is bridged by a binomial form (Ref. 1) similar to the generalized mean (Ref. 5, p. 10).

The report is organized as follows: Chapter 2.0 develops the extinction formula. This includes Sections 2.1, small particle scattering, 2.2 anomalous diffraction, 2.3 the edge effects and 2.4 the binomial bridging function. Chapter 3 and the Appendix contain extensive comparisons of this approximation to the T-matrix method (Ref. 6). The final chapter, Chapter 4., gives the conclusions and remaining limitations.

This work was performed at DREV between October 1990 and March 1992 under PSC 32A, EO/IR Protection of Land Vehicles.

2.0 DEVELOPMENT OF THE EXTINCTION FORMULA

The physics and the structure of the extinction formula for randomly oriented spheroids will be developed in this chapter.

2.1 Small Particle Term

For a physically and optically small particle, all applied electric field gradients disappear and the particle begins to respond to a homogeneous field. The electrostatics approximation then holds, giving rise to the Rayleigh scattering formula for randomly oriented spheroids (Ref. 7). If the particle is still geometrically small but optically large, the magnetic dipole field becomes significant. We have found (Ref. 2) that one can use the electrostatics approximation but with the optical constants transformed. This transform correctly describes the full field. It is exact for spheres and approximate for randomly oriented spheroids. The following formulæfor the extinction efficiency from small particles, Q_{small} are derived in Ref. 2:

$$Q_{small} = Q_{sca} + Q_{abs} \qquad [1]$$

with

$$\begin{aligned} Q_{sca} &= \frac{16}{9}\frac{b^4 r^2}{\overline{A}}\left\{|\tilde{\eta}_1|^2 + |\tilde{\eta}_1'|^2 + 2\left(|\tilde{\eta}_2|^2 + |\tilde{\eta}_2'|^2\right)\right\} \qquad \text{and} \\ Q_{abs} &= \frac{8}{3}\frac{br}{\overline{A}}\mathrm{Re}\left\{i\left[\tilde{\eta}_1 + \tilde{\eta}_1' + 2\left(\tilde{\eta}_2 + \tilde{\eta}_2'\right)\right]\right\} \end{aligned} \qquad [2]$$

where

$$\tilde{\eta}_i = \frac{1}{3(L_i + \frac{1}{\mathcal{E}_{1i}-1})}, \quad \tilde{\eta}_i' = \frac{1}{3(L_i + \frac{1}{\mathcal{U}_{1i}-1})}. \qquad [3]$$

The optical constants transform is

$$\mathcal{E}_{1i} = \epsilon\left[\frac{2}{\overline{z}_i}\frac{\psi_1(\overline{z}_i)}{\psi_1'(\overline{z}_i)}\right]^{\zeta}, \quad \text{and} \quad \mathcal{U}_{1i} = \mu\left[\frac{2}{\overline{z}_i}\frac{\psi_1(\overline{z}_i)}{\psi_1'(\overline{z}_i)}\right]^{\zeta}, \qquad [4]$$

where $\psi_1(z)$ is the first Ricatti-Bessel function and

$$\begin{aligned} \overline{z}_1 &= \sqrt{\epsilon\mu}\, b(1+\chi(1-1/r^2)) \qquad \text{prolates} \\ &= \sqrt{\epsilon\mu}\, b(r^2)^{\chi} \qquad \text{oblates} \end{aligned} \tag{5}$$

$$\begin{aligned} \overline{z}_2 &= \sqrt{\epsilon\mu}\, b(1+\chi^{1/3}(1-1/\sqrt{r})) \quad \text{prolates} \\ &= \sqrt{\epsilon\mu}\, b(\sqrt{r})^{\chi^{1/3}} \qquad \text{oblates} \end{aligned} \tag{6}$$

where $\chi \approx \sqrt{3}/10$ and $\zeta \approx \{(91|m-1|-64)/155 \mid 0 \le \zeta \le 1\}$.

The normalization factor is

$$\begin{aligned} \overline{A} &= 1+\frac{r^2}{\sqrt{r^2-1}}\sin^{-1}\left(\frac{\sqrt{r^2-1}}{r}\right) \quad \text{for prolates,} \\ &= 1+\frac{r^2}{\sqrt{1-r^2}}\ln\left(\frac{1+\sqrt{1-r^2}}{r}\right) \quad \text{for oblates.} \end{aligned} \tag{7}$$

The form factors are defined, for prolates as

$$L_1 = \frac{(1-g^2)}{g^2}\Big\{-1+\frac{1}{2g}\ln\Big(\frac{1+g}{1-g}\Big)\Big\}, \quad L_2 = \frac{1-L_1}{2}, \quad g^2 = 1-\frac{1}{r^2} \tag{8}$$

and for oblates,

$$L_1 = \frac{1+f^2}{f^2}\Big\{1-\frac{\tan^{-1}f}{f}\Big\}, \quad L_2 = \frac{1-L_1}{2}, \quad f^2 = \frac{1}{r^2}-1. \tag{9}$$

The above set of equations is identical to that found in Ref. 2 apart from the exponent ζ in [4]. This exponent is introduced for the following reason. The exact solution of the scattering problem can be expressed in terms of scattering coefficients (for spheres,

these are the Mie coefficients). For small physical sizes the first scattering coefficient is dominant and can be expanded as an infinite power series in the size parameter x. The first term of this series is dominant only when $|m-1|$ is small. If we transform the optical constants then the first scattering coefficient can still be expressed as an infinite series in x, but this time the first term dominates only when $|m-1|$ is large. For intermediate values of $|m-1|$, more terms of the power expansion of the scattering coefficients are required. Since the resulting expression would be cumbersome we have decided to modify the first term of the transformed series in such a way as to model empirically the scattering behaviour from small to large $|m-1|$. A simple and robust way to achieve this is to gradually turn on the transform by using the exponent ζ. Thus when $\zeta = 0$ the Rayleigh expression results and when $\zeta = 1$ the fully transformed expression results. Note that $\zeta = 0$ when $|m-1| \leq 64/91 \approx 0.7$ and $\zeta = 1$ when $|m-1| \geq 219/91 \approx 2.4$.

2.2 Large Particle Term

In this section we discuss the extinction efficiency of large particles Q_{large}. We separate the physics into two parts, one which corresponds to the anomalous diffraction, Q_{ad}, and the other, which can be considered due to edges effects, Q_{ed}.

2.2.1 Extended Anomalous Diffraction

The anomalous diffraction formula is derived (Refs. 1 and 8) by assuming that the incident plane wave is not significantly skewed in passing through the scattering object and that, to first order, the effect of the scatterer is to locally delay the phase of the wave and attenuate its amplitude (Ref. 3). The strict limit of validity of the formula is therefore the region where $(n-1) << 1$. The scattering object is in effect treated as an irregular disc normal to the incident wave possessing a spatially dependent phase and amplitude. The Fraunhofer pattern at infinity is then derived and Q_{ext} evaluated from the standard relations. For a spheroidal scatterer, this procedure leads immediately to the following formula :

$$Q_{ad} = \mathrm{Re}\left\{2 + 4\frac{e^{-\omega}}{\omega} + 4\frac{(e^{-\omega}-1)}{\omega^2}\right\} \qquad [10]$$

where ω is given by

$$\omega = i\Delta\psi, \qquad \Delta\psi = 2(m-1)\frac{rb}{p} \qquad [11]$$

and

$$p = \sqrt{\cos^2\theta + r^2\sin^2\theta}, \qquad a = 2\pi\alpha/\lambda, \qquad b = 2\pi\beta/\lambda, \qquad m = n - ik. \qquad [12]$$

Where $r = a/b$ is the aspect ratio (for prolates $r > 1$ and for oblates $r < 1$), α is the length of the semi-axis of rotation, β is the other axis of the spheroid, θ is the angle between the incident radiation and the α or a axis, and λ is the wavelength of the scattered radiation. Hence a and b are the two size parameters associated with the spheroid, and p can be considered a projection operator of the penumbral ellipse (the ellipse defined by the shadow

line on the surface of the spheroid) onto the plane perpendicular to the direction of the incoming radiation. When compared with exact results this formulation is satisfactory for all oblate spheroids. For prolates, however, significant phase differences appear due to deviation of the central ray.

To account for the refraction of the central ray, we have previously modified the anomalous diffraction approximation (Ref. 1). The deviation of the central ray is now taken into account when computing its phase difference.

The extended anomalous diffraction $\Delta\psi$ is found to be

$$
\begin{aligned}
w = i\Delta\psi &= ib\left\{\frac{2r}{p}\left[\frac{p^2\cos(\phi)+s\sin(\phi)}{p^2\cos^2(\phi)+q^2\sin^2(\phi)+2s\cos(\phi)\sin(\phi)}\right]\right\}(m-\cos(\phi)) \\
\cos(\phi) &= \frac{s^2+p^2\Delta}{m(p^4+s^2)} \\
\sin(\phi) &= \frac{s(\Delta-p^2)}{m(p^4+s^2)} \\
\Delta &= [m^2(p^4+s^2)-s^2]^{1/2} \\
s &= \sqrt{p^2q^2-r^2} \\
q &= [r^2\cos^2(\theta)+\sin^2(\theta)]^{1/2}.
\end{aligned}
\qquad [13]
$$

In the limiting cases of $r \to \infty$ $\Delta\psi$ becomes:

$$\Delta\psi = 2b\{(m^2-\cos^2\theta)^{1/2}-\sin\theta\}. \qquad [14]$$

For random orientations the angular averaging is carried out as follows:

$$\overline{Q}_{ad} = \frac{\int_0^{\pi/2} Q_{ad} p \sin\theta\, d\theta}{\int_0^{\pi/2} p\sin\theta\, d\theta} \qquad [15]$$

The integration in the numerator of [15] can be readily computed numerically if the kernel is not too oscillatory. However, [15] can be analytically approximated by the technique described in Ref. 9. This eliminates numerical difficulties and leads to a more efficient algorithm. Following the procedure of Ref. 9, [15] becomes:

$$\overline{Q}_{ad} = 2 + 4(I_1 - I_2)/j(0) \qquad [16]$$

with

$$I_1 = A\left[e^{-C}\left\{(1+\frac{1}{C})\frac{F_2(C)}{C} - (1+\frac{2}{C})\frac{F_1(C)}{C^2}\right\} + (1+\frac{2}{C})\frac{F_1(0)}{C^2} + \frac{F_2(0)}{C^2}\right] \qquad [17]$$

and

$$I_2 = \frac{j(0)}{C^2} + \frac{A}{C^2}(\frac{1}{\omega(0)} - \frac{1}{\omega(\pi/2)}) + \frac{2A}{C^3}\ln\left[\frac{B\omega(\pi/2)}{(B+j(0))\omega(0)}\right] \qquad [18]$$

where

$$\begin{aligned} A &= \gamma B[B + j(0)], \qquad B = \frac{\omega(0) - \omega(\pi/4)}{\gamma + [\omega(\pi/4) - \omega(\pi/2)]/j(\pi/4)}, \\ C &= \omega(0) - \gamma B, \qquad \gamma = \frac{\omega(\pi/2) - \omega(0)}{j(0)}, \end{aligned} \qquad [19]$$

and

$$\begin{aligned} j(\theta) &= -\frac{1}{2}\left[\cos(\theta)\sqrt{1 - g^2\cos^2(\theta)} + \frac{\sin^{-1}(g\cos(\theta))}{g}\right], \qquad \text{for prolates,} \\ &= \frac{r}{2}\left[\cos(\theta)\sqrt{1 + f^2\cos(\theta)^2} + \frac{\ln(f\cos(\theta) + \sqrt{1 + f^2\cos(\theta)^2})}{f}\right], \qquad \text{for oblates.} \end{aligned} \qquad [20]$$

Also,

$$F_n(C) \equiv \frac{E_n(\omega(0) - C)}{(\omega(0) - C)^{n-1}} - \frac{E_n(\omega(\pi/2) - C)}{(\omega(\pi/2) - C)^{n-1}}, \qquad [21]$$

where E_n is the nth order exponential integral (Ref. 5). And finally for prolates (considering deviated rays),

$$\begin{aligned}
\omega(0) &= 2bi\left[\frac{\sqrt{m^2-1}\,(m-1)}{(1-\alpha)(m-1)+\alpha\sqrt{m^2-1}/r}\right], \\
\omega(\pi/4) &= 2bi\left[g^2(\sqrt{m^2-1/2}-1/\sqrt{2})+\frac{m-1}{r^2}\right], \\
\omega(\pi/2) &= 2bi(m-1), \\
\frac{1}{\alpha} &= 1-rc\frac{(1-r)}{(1-rc)}, \quad rc=\sqrt{\left|\frac{m-1}{m+1}\right|},
\end{aligned} \tag{22}$$

for oblates (undeviated rays),

$$\begin{aligned}
\omega(0) &= 2br\,i(m-1), \\
\omega(\pi/4) &= 2br\,i(m-1)\sqrt{\frac{2}{1+r^2}}, \\
\omega(\pi/2) &= 2bi(m-1).
\end{aligned} \tag{23}$$

As a consequence of the analytic integration technique, [13] is approximated by [22] at three values of θ whereas [11] exactly reduces to [23] at the same three values. Note that [16] can be shown to reduce to the anomalous diffraction formula of Van de Hulst for the sphere.

2.2.2 Edge Effects

For a particle whose typical size is much larger than the wavelength, the edge cannot be treated as sharp and the effect of the curvature of the object must be included.

Jones (Ref. 4) has shown how to estimate these edge effects for three dimensional convex bodies. In Ref. 1 we showed that

$$\begin{aligned} Q_{edge} &= \frac{2Dr^{2/3}}{p^{2/3}}\,{}_2F_1(-2/3,1/2;1;(1-1/p^2)) \quad \text{(prolates)} \\ &= \frac{2Dr^{2/3}}{p^{2}}\,{}_2F_1(-2/3,1/2;1;(1-p^2)) \quad \text{(oblates)}, \end{aligned} \tag{24}$$

$${}_2F_1(-2/3,1/2;1;z) \approx \frac{.999947 - 2.19081z + 1.51871z^2 - .325449z^3}{1 - 1.85884z + .947705z^2 - .0847327z^3}, \qquad |z| \le 1,$$

$$D = c_e/b^{2/3}. \tag{25}$$

It can be shown for convex bodies, randomly oriented or illuminated by a randomly polarized beam, that c_e is a universal function of m. As $|m-1| \to 0$, $c_e \to c_0 = 0.996130$ and as $|m-1| \to \infty$, $c_e \to c_\infty = 0.0659708$ (Refs. 1, 11 and 12). This universal function is not known and therefore must be modelled. Since c_e is independent of shape, this can be accomplished by studying the sphere alone. An added complication to D arises, however, when we consider spheroids with small phases, i.e. $\Delta\psi << 1$. This occurs since what we have been calling an edge effect is in fact the field distortion around the boundaries of the particle, and hence its behaviour for small $\Delta\psi$ is quite different than for large $\Delta\psi$. As before, we have modelled this effect in our expression for D by using the sphere. Our empirical model of the above two behaviours is:

$$\begin{aligned} D &= \frac{c_o}{[b^{2\beta/3} + 1/|m-1|^{\beta}]^{1/\beta}} \\ \beta &= \frac{4/25}{|m-1|^3 + 8/125} + \left|\frac{c_o - c_\infty}{\ln|m-1|}\right|, \qquad |m| \le 1.95 \quad \text{or} \quad |m| \ge 2.05 \\ &= 20, \qquad\qquad 1.95 < |m| < 2.05 \end{aligned} \tag{26}$$

In the above, the special case for β with $m \approx 2$ is to avoid the obvious singularity in the main expression. At this point we require only a relatively large value for β.

The large particle limit for the spheroid becomes

$$Q_{ext} \rightarrow 2 + Q_{edge}. \qquad [27]$$

We now wish to produce a term T which, when it multiplies [10], gives the same limit as [27] without diverging as the size parameter goes to zero. We have found that (Ref. 1) an adequate expression for our purposes is:

$$T = 2 - e^{-Q_{edge}/2} \qquad [28]$$

For random orientations the angular averaging is carried as in [15] but with T replacing Q_{ad}:

$$\overline{T} = \frac{\int_0^{\pi/2} T p \sin\theta \, d\theta}{\int_0^{\pi/2} p \sin\theta \, d\theta} \qquad [29]$$

Using the same integration technique to obtain an analytic approximation to [29] we obtain:

$$\overline{T} = 2 - e^{-\delta C'} A' F_2' / j'(0) \qquad [30]$$

where

$$\begin{aligned} A' &= \gamma' B' [B' + j'(0)], \quad B' = \frac{1 - v(\pi/4)}{\gamma' + [v(\pi/4) - v(\pi/2)]/j'(\pi/4)}, \\ C' &= 1 - \gamma' B', \quad \gamma' = \frac{v(\pi/2) - 1}{j'(0)}, \quad \delta = D r^{2/3}. \end{aligned} \qquad [31]$$

and

$$F_2' \equiv \frac{E_2(\delta)}{\delta} - \frac{E_2(\delta v(\pi/2))}{\delta v(\pi/2)}. \qquad [32]$$

Here E_2, is the 2nd order exponential integral. For prolates,

$$\begin{aligned} j'(\theta) &= rj(\theta), \\ v(\pi/4) &= {}_2F_1[-\frac{2}{3},\frac{1}{2};1;(r^2-1)/(r^2+1)][2/(r^2+1)]^3 \\ v(\pi/2) &= {}_2F_1[-\frac{2}{3},\frac{1}{2};1;1-1/r^2]/r^{2/3} \end{aligned} \quad [33]$$

and for oblates,

$$\begin{aligned} j'(\theta) &= -j(\theta), \\ v(\pi/4) &= {}_2F_1[-\frac{2}{3},\frac{1}{2};1;1-r^2/2]/r \\ v(\pi/2) &= {}_2F_1[-\frac{2}{3},\frac{1}{2};1;1-r^2]/r^2 \end{aligned} \quad [34]$$

2.2.3 Total Contribution to Q_{large}

The total contribution to Q_{large} for a given orientation is (Ref. 1):

$$Q_{large} = Q_{ad}T. \quad [35]$$

For random orientation the angle averaging would give:

$$\overline{Q}_{large} = \frac{\int_0^{\pi/2} Q_{ad}Tp\sin\theta\, d\theta}{\int_0^{\pi/2} p\sin\theta\, d\theta}. \quad [36]$$

Due to their complementary nature, $Q_{ad} \approx 2 = \text{constant}$ for large $|\omega|$ while $T \approx \text{constant}$ for small to medium $|\omega|$. Therefore, to a good approximation, we can separate the kernel of the above integral to obtain:

$$\overline{Q}_{large} = \overline{Q}_{ad}\overline{T}. \quad [37]$$

An extensive comparison between [37] and the numerical computation of $\overline{Q}_{large}$ from [36] provides definitive evidence for the above argument. Some examples of this are shown in the next chapter.

2.3 Bridging Function

$\overline{Q}_{small}$ is a good approximation to $\overline{Q}_{ext}$ when the semi-major axis is less than 1. For larger values of the semi-major axis it overestimates $\overline{Q}_{ext}$. Similarly, $\overline{Q}_{large}$ is a good approximation to $\overline{Q}_{ext}$ when the semi-major axis is greater than $2-5$ depending on $|m-1|$. For smaller values of the semi-major axis it overestimates $\overline{Q}_{ext}$. To obtain $\overline{Q}_{ext}$ in the transition region from $\overline{Q}_{large}$ and $\overline{Q}_{small}$, we need a bridging function that smoothly goes between the two. The form must have $\overline{Q}_{small}$ as the first term in its series expansion and asymptotically go to $\overline{Q}_{large}$.

A quite general form that can do this is the confluent hypergeometric function or Kummer function which has the general form ${}_1F_1[a;b,cz^\nu]$, where a, b, c, ν are arbitrary parameters and z is the variable (Ref. 5). From the basic properties of this function

$$\lim_{z\to 0} \frac{\Gamma(b-a)}{\Gamma(b)} c^a z^{a\nu} {}_1F_1[a;b,-cz^\nu] \;\rightarrow\; \frac{\Gamma(b-a)}{\Gamma(b)} c^a z^{a\nu} \left\{ 1 - \frac{caz^\nu}{b} + \frac{ba(a+1)z^{2\nu}}{2!\,b(b+1)} - \ldots \right\}$$

$$\lim_{z\to \infty} \frac{\Gamma(b-a)}{\Gamma(b)} c^a z^{a\nu} {}_1F_1[a;b,-cz^\nu] \;\rightarrow\; 1 + \frac{a(1+a-b)}{cz^\nu} + \ldots \qquad [38]$$

With the small and large particle limits considered the bridging function $\mathcal{B}$ becomes:

$$\mathcal{B} \;\equiv\; \overline{Q}_{small} \cdot F_1[1/\nu; b; -(cz)^\nu] \quad \text{with}$$

$$c = \Gamma(b)/\Gamma(b-1/\nu), \quad \text{and} \quad z = \overline{Q}_{small}/\overline{Q}_{large} \tag{39}$$

which has the correct limits, i.e.

$$\begin{aligned} \lim_{z\to 0} \mathcal{B} &\rightarrow \overline{Q}_{small} \\ \lim_{z\to \infty} \mathcal{B} &\rightarrow \overline{Q}_{large} \end{aligned} \tag{40}$$

We now need to determine ν and b. We should expect these parameters to be insensitive to aspect ratio since most of the shape effects are already accounted for by $\overline{Q}_{small}$ and $\overline{Q}_{large}$. We have confirmed this supposition by numerical evidence. Assuming these parameters are shape independent, we can, for each of an array of m values, find the 'best' set of values of ν and b by considering the sphere only. We did this by using a nonlinear fitting routine. The results of this fit, for the vast majority of cases made b very large (> 10). When b becomes very large, $\mathcal{B}$ goes confluent (see Ref. 13 for more details). This means that the function simplifies dramatically to a binomial function, thus:

$$\lim_{b\to\infty} \mathcal{B} \rightarrow \frac{\overline{Q}_{small}}{[1+z^{\nu}]^{1/\nu}} \tag{41}$$

This can be rearranged in a form similar to a generalized mean as:

$$\frac{1}{\overline{Q}_{ext}^{\gamma}} = \frac{1}{\overline{Q}_{small}^{\gamma}} + \frac{1}{\overline{Q}_{large}^{\gamma}} \tag{42}$$

We must now model the values for γ. We have modelled this parameter in previous papers (Refs. 1 and 14). This previous modelling is not useful to the current approach since $\overline{Q}_{small}$ and $\overline{Q}_{large}$ have changed, the formula for $\overline{Q}_{ext}$ has been extended to all $n \geq 1$ and angle averaging has been carried out.

In [42] if one of either $\overline{Q}_{small}$ or $\overline{Q}_{large}$ is much smaller than the other then, to a good approximation, $\overline{Q}_{ext}$ is this value provided that $\gamma > 0$. Larger values of γ will drive $\overline{Q}_{ext}$ to the smallest value between $\overline{Q}_{small}$ and $\overline{Q}_{large}$ more than smaller values. When the physical size of the particle is small, $\overline{Q}_{small}$ is equal to or less than $\overline{Q}_{large}$ and hence γ should be large. Conversely, when the physical size of the particle is large, $\overline{Q}_{small}$ is much larger than $\overline{Q}_{large}$ and we then merely require that γ be positive. The real difficulty in modelling γ is thus in the intermediate ranges of physical sizes. Most of the behaviour of γ in the large particle regime can be determined by considering first the real axis, in the refractive index plane, and then by varying the imaginary component. Considering first the real axis, the behaviour can be described by the sum of two asymptotic terms, one as $n - 1 \rightarrow 0$ and the other as $n \rightarrow \infty$. The behaviour of γ as k increases is well modelled by a single term. The sum of these terms we will call γ_l. As the physical size of the particle changes from small to large, γ must go smoothly from some large value to γ_l. This transition is most sensitive, and hence best modelled, where the Rayleigh scattering and absorption are roughly equal. This occurs since the Rayleigh absorption term and the anomalous diffraction absorption term are close to or may be equal while the scattering terms are usually quite different. This can play significantly on the balance between $\overline{Q}_{small}$ and $\overline{Q}_{large}$ as the physical size varies. This has been taken into account by an additional term dependent on the physical size. This size is represented by the spherical volume equivalent radius of the spheroid.

From an empirical fit on the above terms, γ becomes:

$$\gamma = \gamma_l + \frac{(54-\gamma_l)}{1+(ar^{1/3}b)^4}, \qquad a = \frac{5}{2} + \frac{3k_c}{k_c+k}, \qquad k_c = \frac{(n^2-1)^2}{66n}$$

$$\gamma_l = 1 + \frac{n-1}{[(n-1)^{1/3}+1]^3} + 4\left[\frac{4n}{\sqrt{16+n^2}} - 1\right]^2 + \frac{16u^2}{\sqrt{u^4+1}}, \qquad u = \frac{k}{[2(n-1)]^2} \quad [43]$$

We have verified that none of the above modelling of γ changes the empirical fact that $\mathcal{B}$ goes confluent in the best fit and hence [42] still remains valid. It should also be pointed out that the bridging function is not necessary if $\overline{Q}_{ext}$ is only required outside the transition region. In this case $\overline{Q}_{ext} = \overline{Q}_{small}$ or $\overline{Q}_{ext} = \overline{Q}_{large}$, depending on the region of interest.

3.0 RESULTS

The complete formula, as presented in the previous chapter, gives correct asymptotic behaviour for both large and small $|m-1|$ and b. Thus, in studying the error behavior of the approximation, the mid-ranges of $|m-1|$ and b are of greatest interest. In this chapter we will compare the analytic approximation with the exact T-matrix method as implemented by Barber (Ref. 6) or, for efficiency, the Mie theory when $r = 1$.

Figures 1 and 2 show the comparison of Q_{ext} versus b for aspects 2 and 1/2, respectively. The refractive index is $n = 1.3$, close to that of water. It is clear that the error decreases at either extreme of b. (The deviation seen in Fig. 1 for $b > 23$ is caused by ill conditioning in the T-matrix code). The largest errors are near and around the first two peaks. This occurs since much more of the scattering physics must be considered.

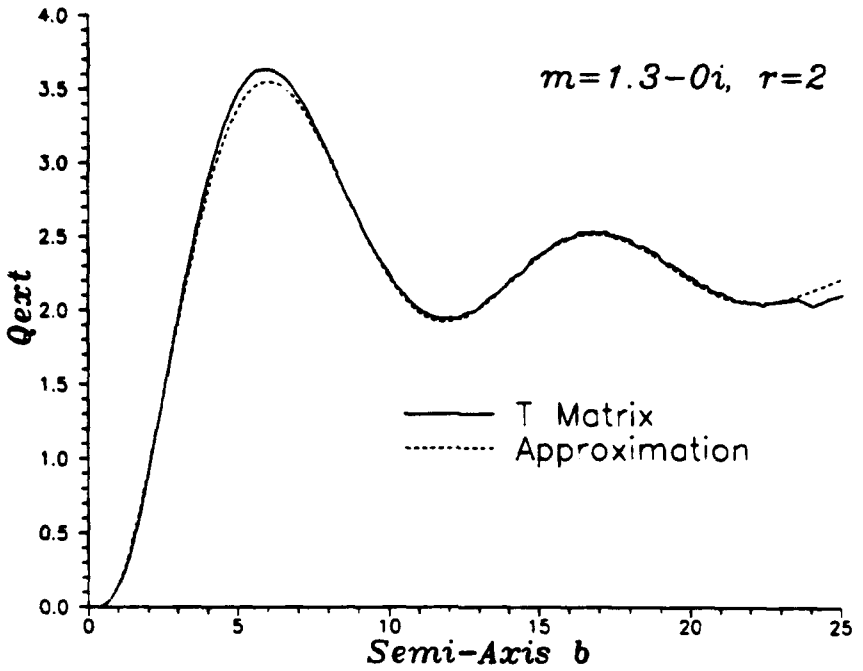

FIGURE 1 – Comparison between approximation and T-matrix method for an index of 1.3 and an aspect ratio of 2

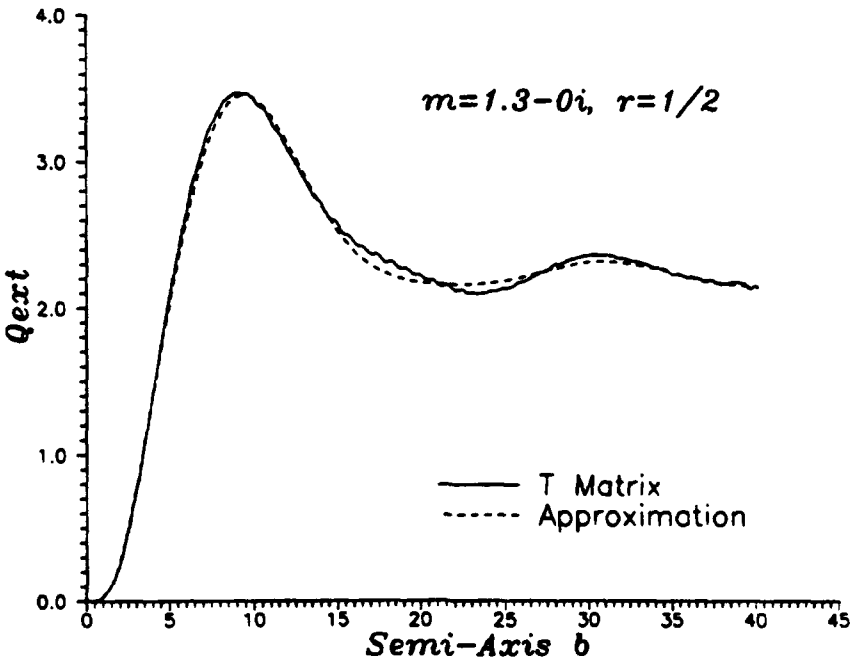

FIGURE 2 – Comparison between approximation and T-matrix method for an index of 1.3 and an aspect ratio of 1/2

Figures 3 and 4 are contour graphs of the percent error between the analytic approximation and the T-matrix computation. The refractive index varies as $1 \leq n \leq 3$ and $10^{-5} \leq k \leq 10$. Figure 3 is for a sphere and Fig. 4 is for a prolate spheroid of aspect 2. There are three features of note. One is the increase of the error for small k and large n. This error is shown well in Fig. 5 for the case of a sphere and index $m = 1.8 - 0\mathrm{i}$. This feature is simply due to resonant surface waves that are not modelled. Note that for aspect 2, these errors are significantly smaller since the surface waves are damped by the asphericity. The remaining errors arise from inaccurate modelling of the bridging region — that is between the Rayleigh region and the first peak. The second feature occurs approximately when $2 < k < 10$. Here, for large particles, the coherence effect of the internal refracted wave is significant and hence has not been properly modelled (Ref. 15). This is shown in Fig. 6 for an oblate particle with an aspect ratio of 1/2 and $m = 1 - 3\mathrm{i}$. This becomes insignificant for larger k since the particle becomes reflective. The remaining error at these large values of k and $b \approx 1$ is again due to difficulties in the bridging function attempting to model the electromagnetic field on the surface. The third significant feature occurs when the Rayleigh scattering and absorption are roughly equal. This occurs since the Rayleigh absorption term and the anomalous diffraction absorption term are close to or may be equal while the scattering terms are usually quite different. This was included in the modelling of γ in the previous chapter by k_c, [43]. Residual errors can still be seen in Figs. 3 and 4 due to imperfect modelling. These errors follow curves with $k \propto (n^2 - 1)^2/n$.

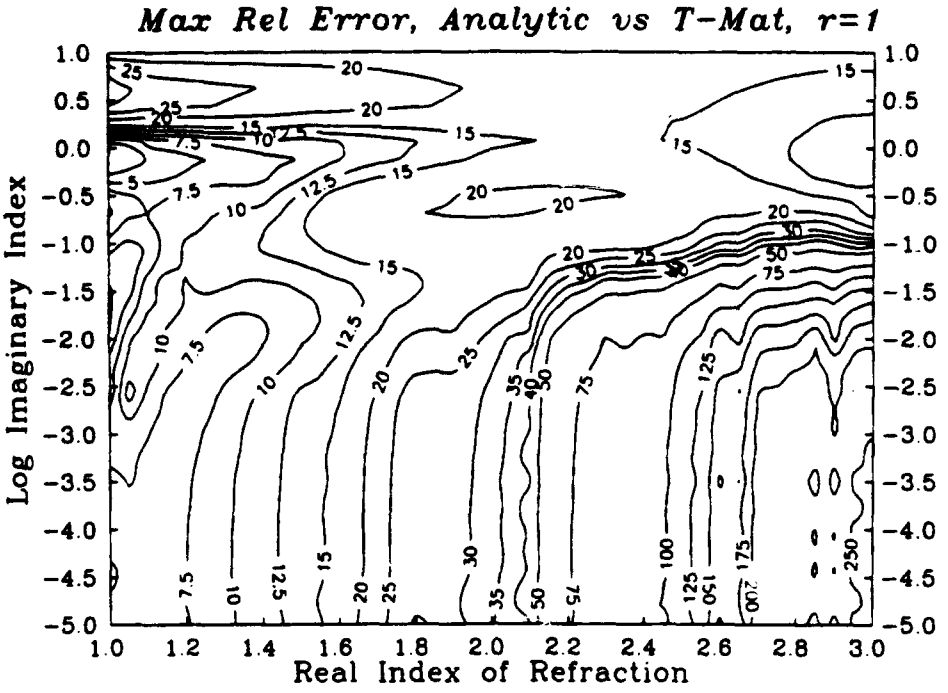

FIGURE 3 – Maximum relative error, in percent, between analytic approximation and Mie theory, $r = 1$

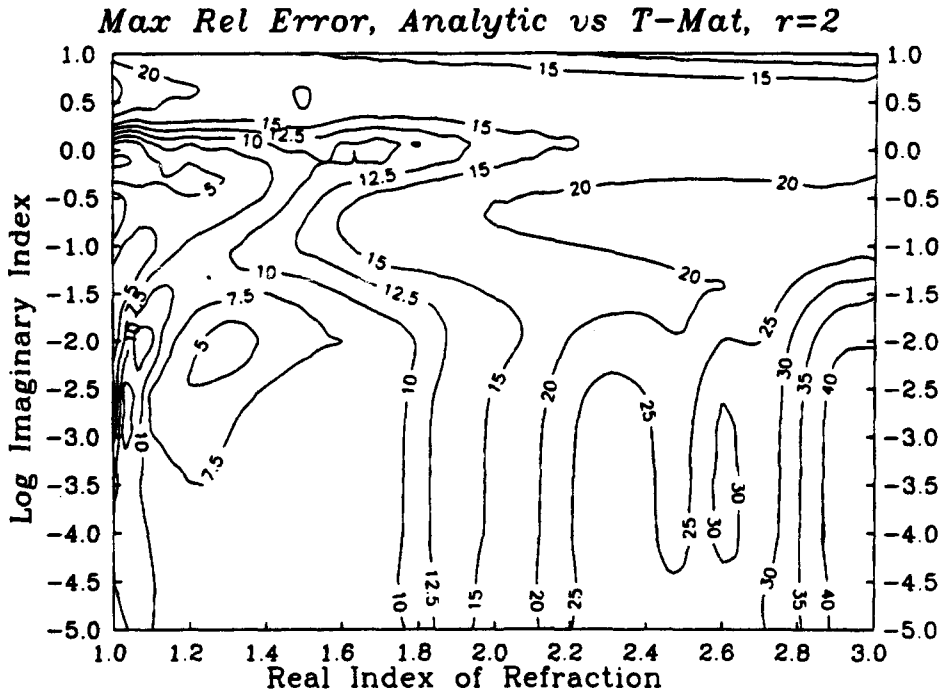

FIGURE 4 – Maximum relative error, in percent, between analytic approximation and T-matrix $r = 2$

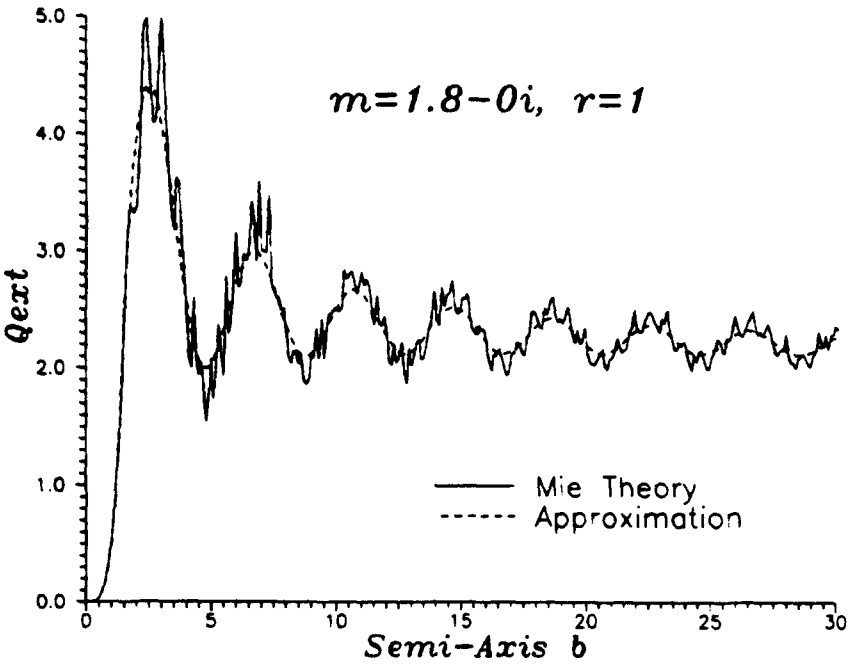

FIGURE 5 – Comparison between approximation and Mie theory for an index of 1.8 and an aspect ratio of 1; significant surface waves.

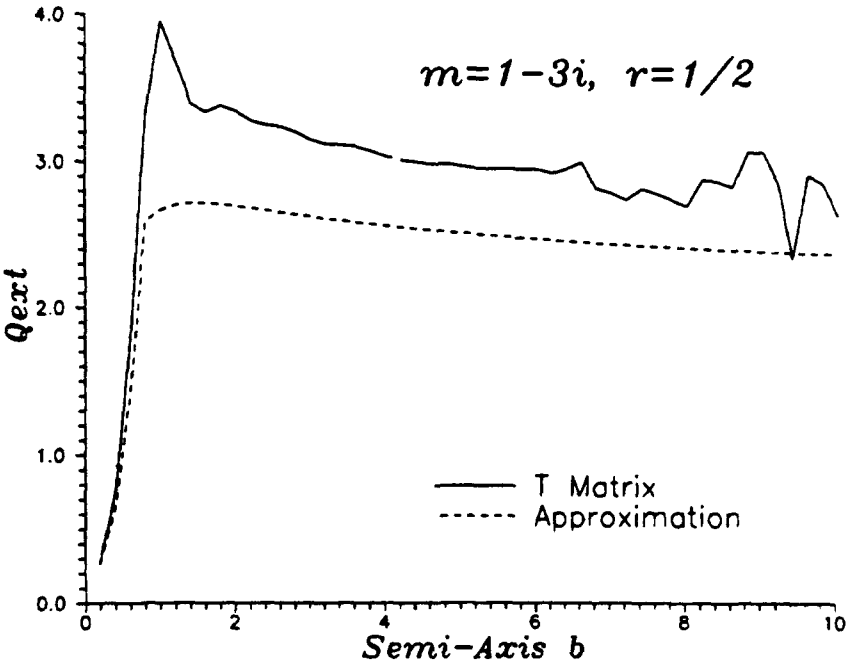

FIGURE 6 – Comparison between approximation and T-matrix method for an index of 1 – 3i and an aspect ratio of 1/2; significant internal wave coherence effect.

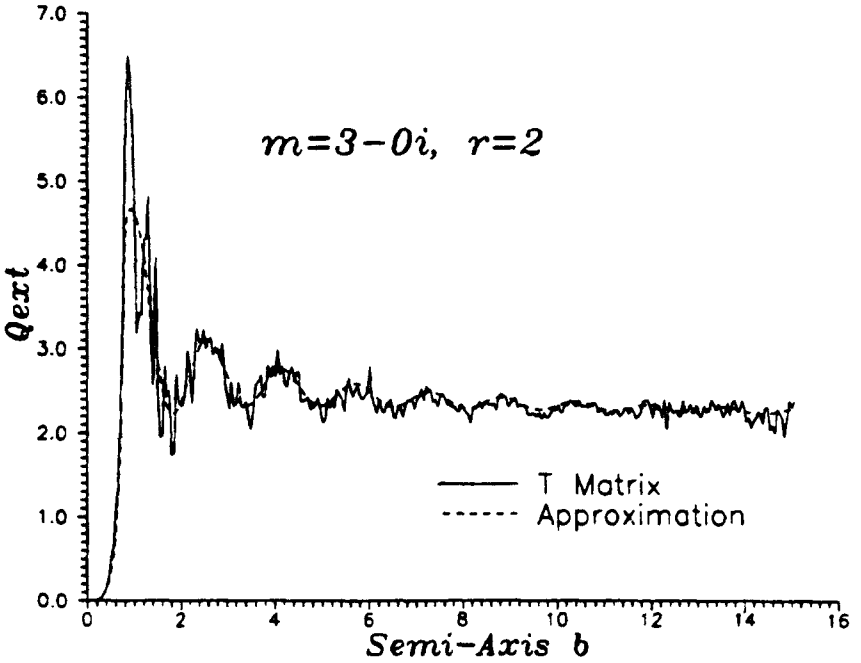

FIGURE 7 – Comparison between approximation and T-matrix method for an index of 3 – 0i and an aspect ratio of 2; incipient MDR at $b \approx 1$

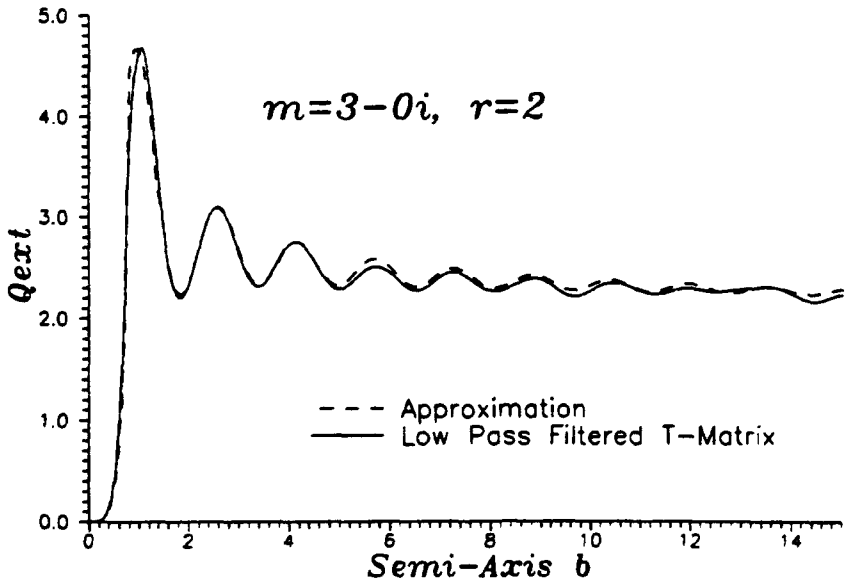

FIGURE 8 – As Fig. 7 but T-matrix results low pass filtered for $b > 1$

For large n, body resonances can occur. These are sometimes called morphology dependent resonances (MDR). For spheres these occur near $nx = l\pi$, where l is a natural number. Figure 7 shows an example of an incipient MDR on the first diffraction peak of Q_{ext}. Here, $m = 3 - 0\,\mathrm{i}$ and $r = 2$. Note that, despite the significant perturbation in the transition region due to the MDR, the approximation is excellent. Only the first, and hence simplest MDRs are modelled (by $\bar{z}_1$, [5] and $\bar{z}_2$, [6]). To show the accuracy of the approximation, the T-matrix was low pass filtered for $b \geq 1$ and is graphed in Fig. 8. Since by far the main contribution is now from the diffraction peaks, the underlying accuracy of the approximation is apparent.

The next example is a model of extinction by randomly oriented copper flakes in the infrared ($m = 35 - 35\,\mathrm{i}$). An oblate spheroid with an aspect ratio of 0.333 was used. For this index, lower aspect ratios could not be considered since the T-matrix will not produce usable results and hence no comparison could be made. Q_{ext} for this case is shown in Fig. 9. Caution is required since the T-matrix for $b > .25$ begins to decrease rapidly and will go negative for larger b. This shows an advantage of the approximation. It can estimate Q_{ext} for combinations of n, k, b and r when the T-matrix cannot. Figures 10 and 11 are examples of Q_{ext} for water prolate and oblates spheroids at 9.4 GHz, respectively. Both are difficult cases since the T-matrix is almost ill conditioned and several MDRs are becoming apparent. In Fig. 10, the first MDR is reasonably well modelled while the second is not. However, the latter only introduces an error of about 20 %. Again Fig. 11, the first MDR is well modelled and the second is not. In contrast to Fig. 10 it introduces a smaller error

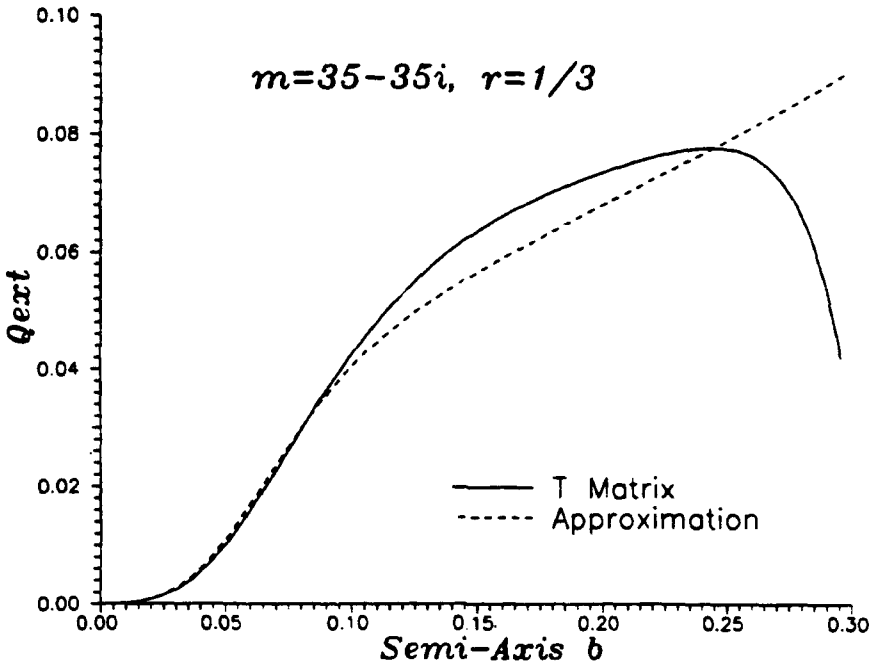

FIGURE 9 – Comparison between approximation and T-matrix method for an index of 35 – 35i and an aspect ratio of 1/3

since it is coincident with the first diffraction peak. Note that at the highest b shown the T-matrix has become ill conditioned.

Extensive computations have been carried out to indicate the error of the approximation over the complete range of stability of the T-matrix method. Both the error and location of the error as a function of refractive index m and aspect ratio r are given in the Appendix.

All our approximate Q_{ext} diagrams in this chapter and the appendix were produced at a rate of greater than 10^4 times faster than by the T-matrix code. Since the T-matrix scales as at least the cube of the optical size whereas the analytic approximation is optical size independent, larger size parameters or larger refractive indices lead to larger speed-up

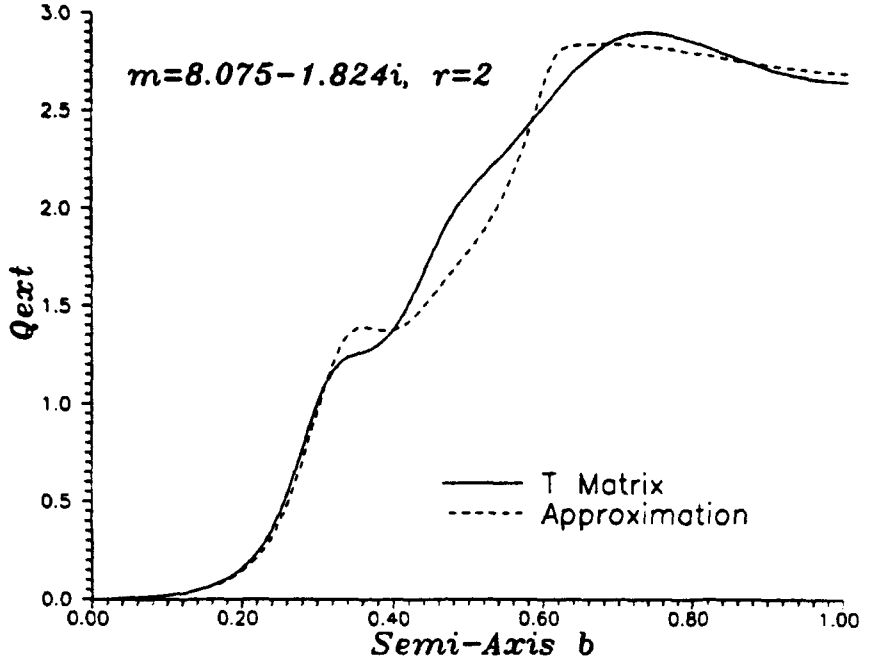

FIGURE 10 – Comparison between approximation and T-matrix method for an index of 8.075 – 1.824i and an aspect ratio of 2; water at 9.4 GHz.

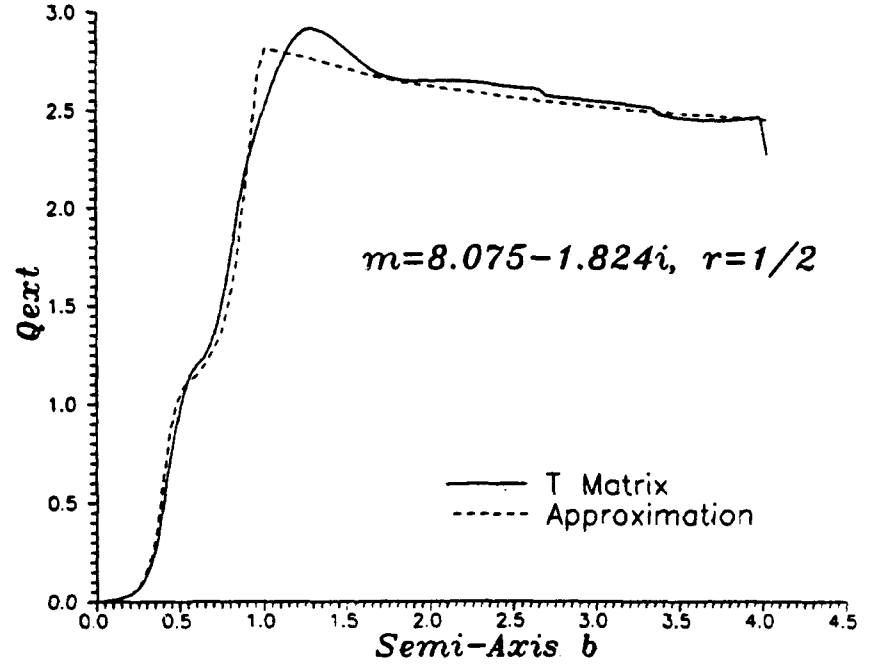

FIGURE 11 – Comparison between approximation and T-matrix method for an index of 8.075 – 1.824i and an aspect ratio of 1/2; water at 9.4 GHz.

factors. For example, letting $m = 1.5$ and $r = 2$, the following execution times on an Intel i860 40 MHz coprocessor are found: 0.25 s, $b = 1$, 4.07 s, $b = 10$ and 2290 s, $b = 75$. Other values of m or r are likely to increase the time. The computation time of the approximation is nearly independent of optical size and aspect ratio and, for the same coprocessor, the execution time is .0029 s. The savings in time is obvious for large b and is still significant for smaller b if many values of Q_{ext} are required.

4.0 CONCLUSIONS AND LIMITATIONS

We have presented an approximation to Q_{ext} for randomly oriented spheroids which gives good results with little loss in accuracy for all size parameters, aspect ratios and refractive indices $n \geq 1$ and $k \geq 0$ and $\mu = 1$. If high precision is not required, the formula is far more economical in computer time than the T-matrix method for obtaining Q_{ext}. When both the range of demonstrated validity and the accuracy are taken into account, this formula is superior to all other approximations known by the authors.

Extensive computations have been carried out to indicate the error of the approximation over the complete range of stability of the T-matrix method. Both the error and location of the error as a function of refractive index m and aspect ratio r are given in the appendix.

Several limitations of the previous numerical approach (Ref. 1) have been removed. The remaining limitations, that for $n < 1$ and/or $k < 0$, are not modelled since new and

significant physical phenomena arise (e.g. total internal reflections and optical gain). Even n modestly less than 1 can cause problems. Another limitation occurs for $2 \leq k \leq 10$ and large particles. In this region, the absorption is not well modelled. If this effect was properly accounted for, Q_{abs} and hence Q_{sca} could be globally and readily obtained by using the same approach.

5.0 ACKNOWLEDGEMENT

The authors would like to thank Dr. Peter Barber of the Clarkson College of Technology for generously making available his T-matrix spheroid code without which this work could not have been carried out.

6.0 REFERENCES

1. Fournier, G.R. and Evans, B.T.N., "Approximation to Extinction Efficiency for Randomly Oriented Spheroids", Applied Optics, Vol. 30, No. 15, p. 2042, 1991.

2. Fournier, G.R. and Evans, B.T.N., "Bridging the Gap Between the Rayleigh and Thomson Limits for Various Convex Bodies", DREV R-4692/93, January, 1993, UNCLASSIFIED.

3. Van de Hulst, H.C., "Light Scattering by Small Particles", 1st Edition, John Wiley & Sons, New York, 1957.

4. Jones, D.S., "High-Frequency Scattering of Electromagnetic Waves," Proc. R. Soc. London, Ser. A 240, p. 206, 1957.

5. Abramowitz, M., Stegun, I.A., Eds., "Handbook of Mathematical Functions", Eighth Dover Edition, New York, 1972.

6. Barber, P.W. and Hill, S.C., "Light Scattering by Particles: Computational Methods", World Scientific, NJ, 1990.

7. Kerker, M., "The Scattering of Light and Other Electromagnetic Radiation," Academic Press, New York, 1969.

8. Greenberg, J.M. and Meltzer, A.S., "The Effect of Orientation of Non-Spherical Particles on Interstellar Extinction", Astrophys. J., Vol. 132, p. 667, 1960.

9. Evans, B.T.N. and Fournier, G.R., "A Procedure for Obtaining an Algebraic Approximation to Certain Integrals", DREV R-4653/91, August, 1991, UNCLASSIFIED.

10. Wolfram, S., "Mathematica: A System for Doing Mathematics by Computer", Addison-Wesley, New York, 1989.

11. Nussenzveig, H.M. and Wiscombe, W.J., "Efficiency Factors in Mie Scattering", Phys. Rev. Lett., 45, p. 1490, 1980.

12. Beckmann, V.P. and Franz, W., "Berechnung der Streuquerschnitte von Kugel und Zylinder unter Anwendung einer modifizierten Watson-Transformation, ", Z. Naturforschg., 12a, p. 533, 1957.

13. Luke, Y.L., "The Special Functions and Their Approximations", Vols. I and II, Academic Press, New York, 1969.

14. Evans, B.T.N. and Fournier, G.R., "A Simple Approximation to Extinction Efficiency Valid Over All Size Parameters", Applied Optics, Vol. 29, 1 November 1990.

15. Cohen, A. and Tirosh, E., "Absorption by a Large Sphere with an Arbitrary Complex Refractive Index", Journal of the Optical Society of America A, Vol. 7, No. 2, pp. 323-325, 1990.

APPENDIX A

Survey of Maximum Relative Error and its Location

An extensive computation of Q_{ext} for $1 \leq n \leq 2$, $10^{-5} \leq k \leq 10$, $1/5 \leq r \leq 5$ and $1/10 \leq rb \leq 30$ was performed using the T-matrix and the analytic approximation. When $r = 1$ a Mie code was used instead. From this calculation the maximum relative error can be deduced. In cases were the error may occur outside the above limits (such as values of m near 1), but still inside the stable region of the T-matrix, the calculation was extended to cover this region. In addition, the value of b were this maximum occured was also recorded.

The sequence of following diagrams gives the results of this computation. The upper diagram is the maximum relative error in percent and the lower diagram is the location of the maximum. Care was taken to insure that the T-matrix was stable. This is done by verifying the convergence of the T-matrix itself where possible, by comparing the backscatter efficiency with the Fresnel coefficient estimate, and with the Rayleigh formula. Since it is difficult estimate the accuracy near the limit of stability of the T-matrix code some additional error due to the T-matrix code could be present.

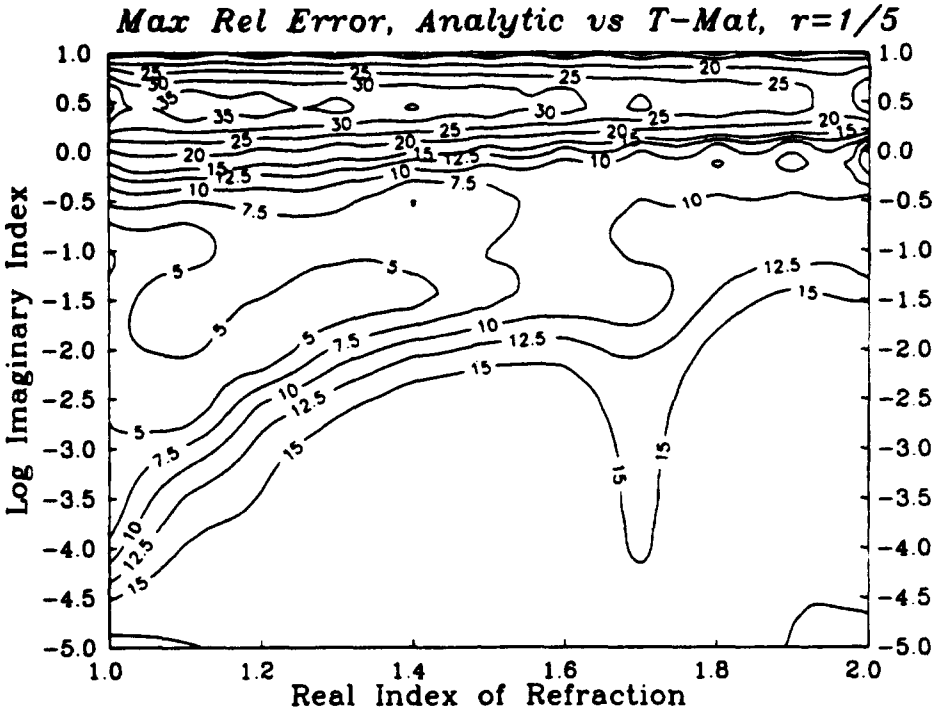
Max Rel Error, Analytic vs T-Mat, r=1/5
Log Imaginary Index
Real Index of Refraction
1.0
0.5
0.0
-0.5
-1.0
-1.5
-2.0
-2.5
-3.0
-3.5
-4.0
-4.5
-5.0
1.2
1.4
1.6
1.8
2.0

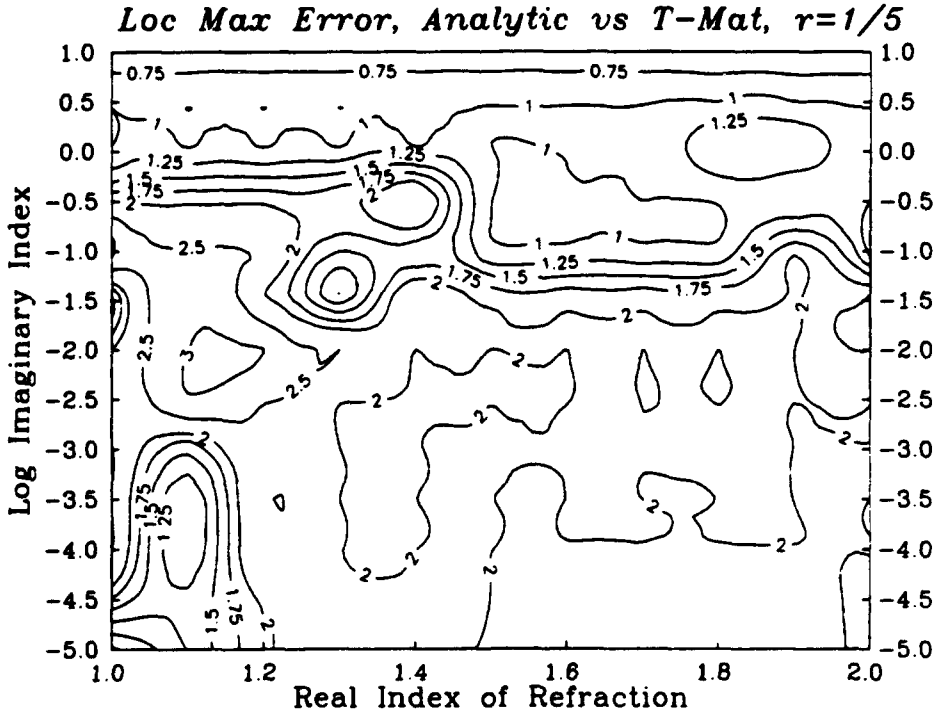
Loc Max Error, Analytic vs T-Mat, r=1/5
Log Imaginary Index
Real Index of Refraction
1.0
0.5
0.0
-0.5
-1.0
-1.5
-2.0
-2.5
-3.0
-3.5
-4.0
-4.5
-5.0
1.2
1.4
1.6
1.8
2.0

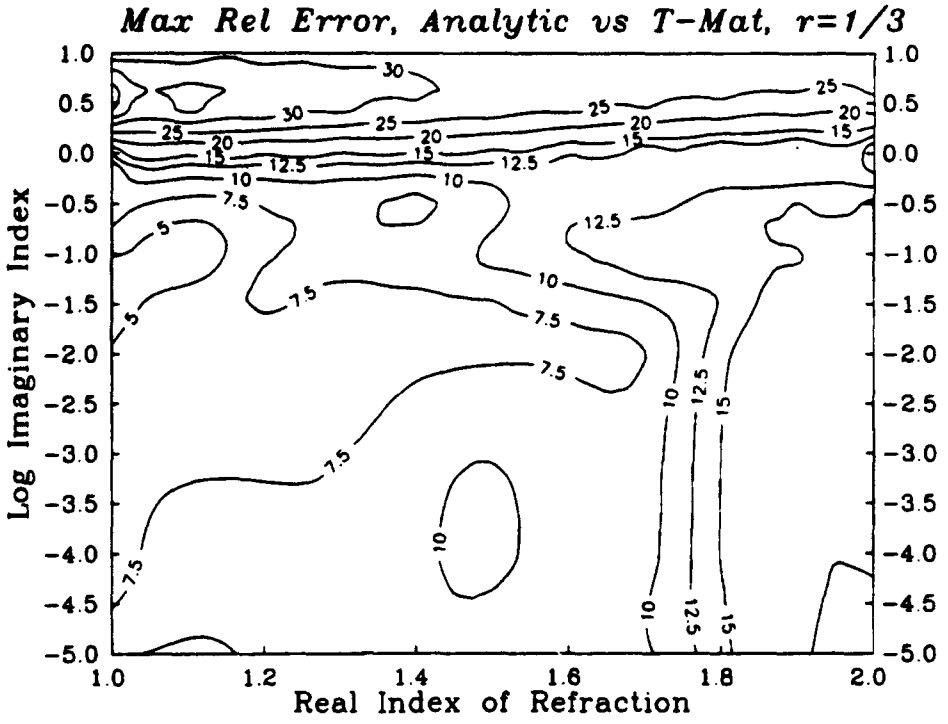
Max Rel Error, Analytic vs T-Mat, r=1/3
Log Imaginary Index
Real Index of Refraction
1.0
0.5
0.0
-0.5
-1.0
-1.5
-2.0
-2.5
-3.0
-3.5
-4.0
-4.5
-5.0
1.2
1.4
1.6
1.8
2.0

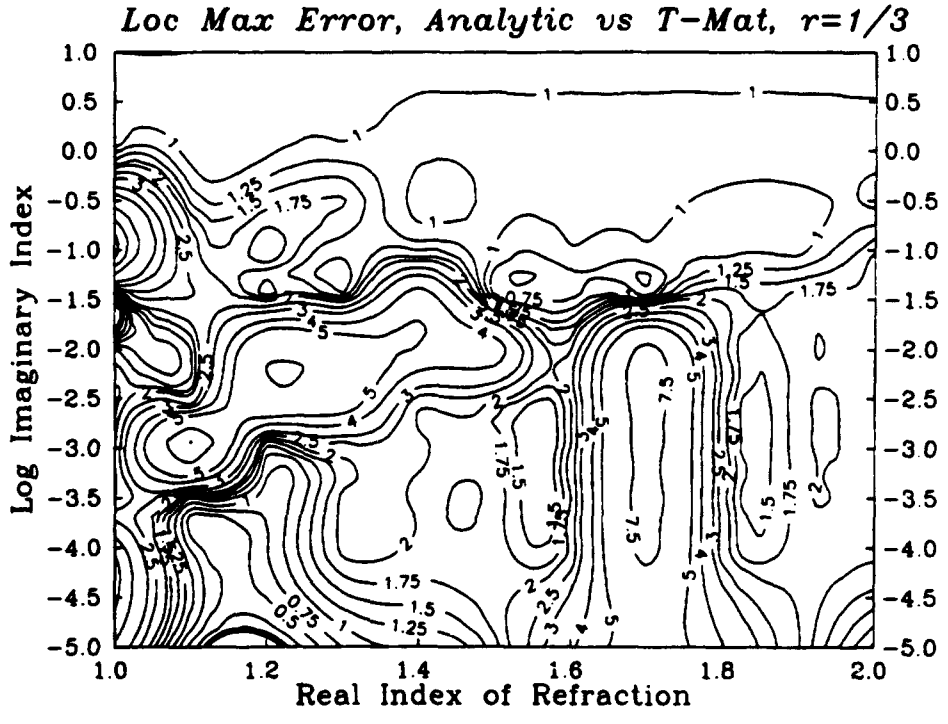
Loc Max Error, Analytic vs T-Mat, r=1/3
Log Imaginary Index
Real Index of Refraction
1.0
0.5
0.0
-0.5
-1.0
-1.5
-2.0
-2.5
-3.0
-3.5
-4.0
-4.5
-5.0
1.2
1.4
1.6
1.8
2.0

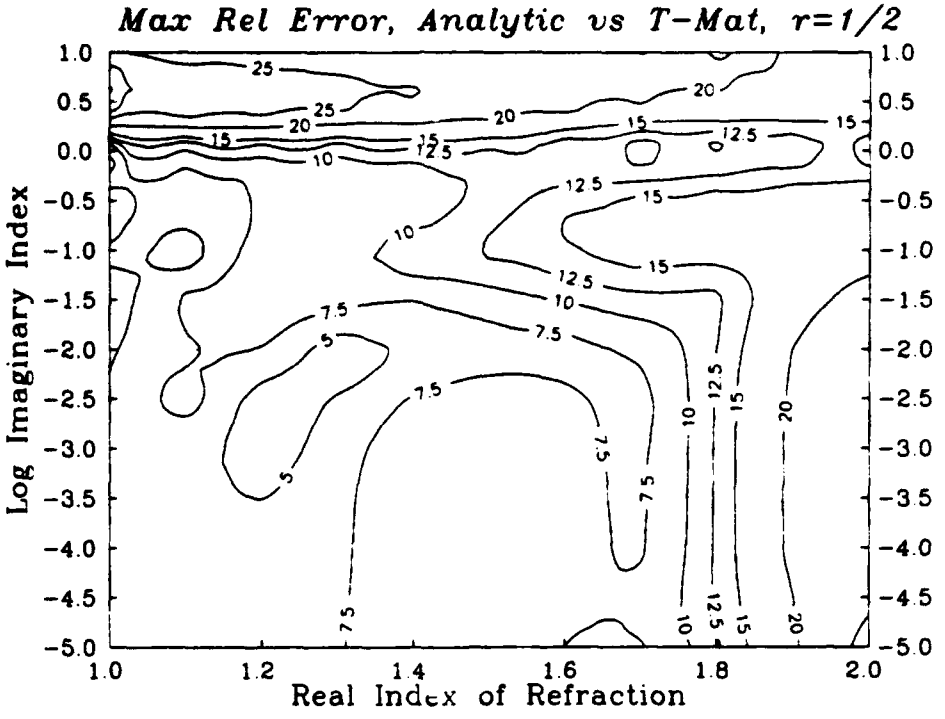
Max Rel Error, Analytic vs T-Mat, r=1/2
Log Imaginary Index
Real Index of Refraction
1.0
0.5
0.0
-0.5
-1.0
-1.5
-2.0
-2.5
-3.0
-3.5
-4.0
-4.5
-5.0
1.2
1.4
1.6
1.8
2.0

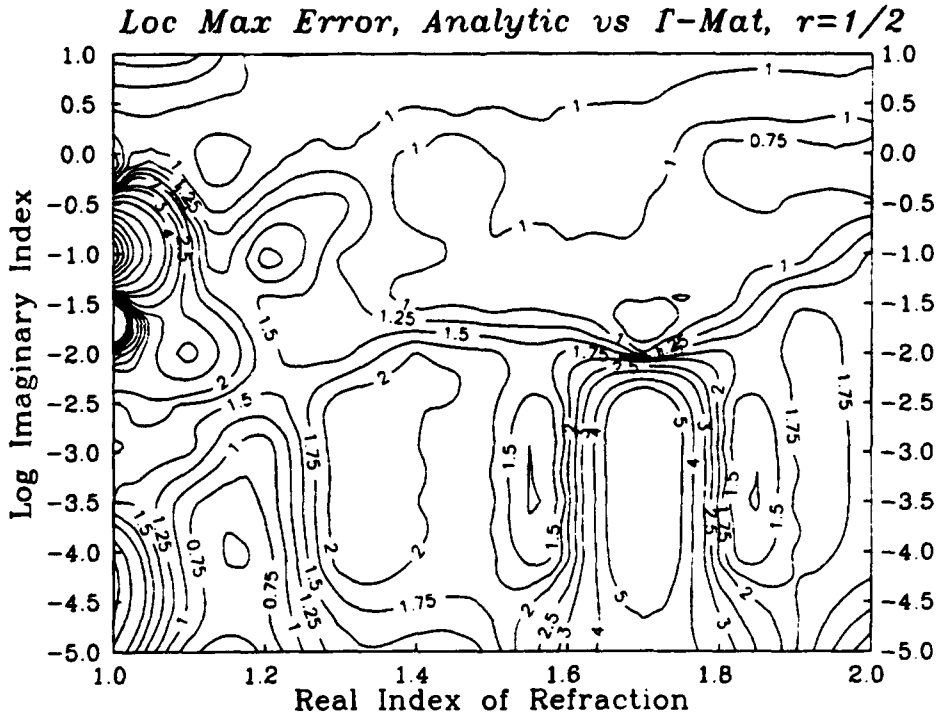
Loc Max Error, Analytic vs T-Mat, r=1/2
Log Imaginary Index
Real Index of Refraction
1.0
0.5
0.0
-0.5
-1.0
-1.5
-2.0
-2.5
-3.0
-3.5
-4.0
-4.5
-5.0
1.2
1.4
1.6
1.8
2.0

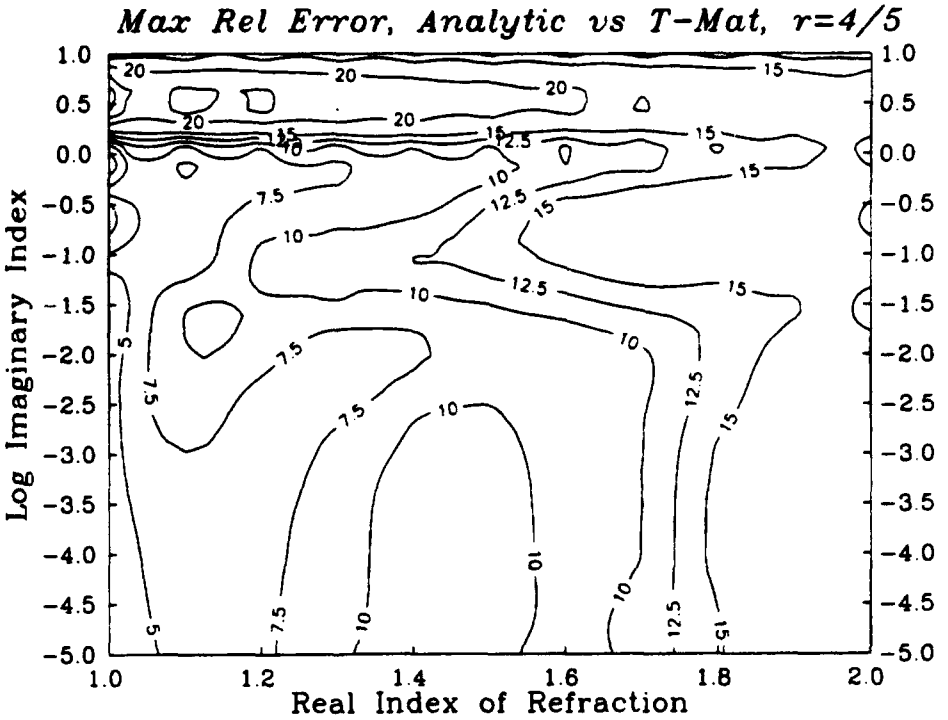
Max Rel Error, Analytic vs T-Mat, r=4/5
Log Imaginary Index
Real Index of Refraction
1.0
0.5
0.0
-0.5
-1.0
-1.5
-2.0
-2.5
-3.0
-3.5
-4.0
-4.5
-5.0
1.2
1.4
1.6
1.8
2.0

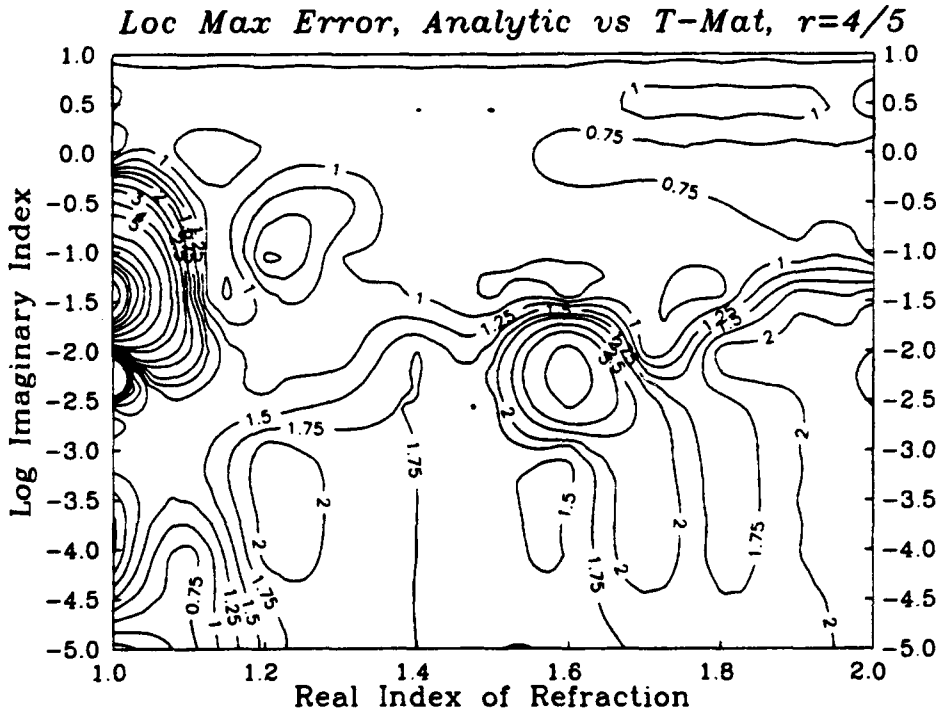
Loc Max Error, Analytic vs T-Mat, r=4/5
Log Imaginary Index
Real Index of Refraction
1.0
0.5
0.0
-0.5
-1.0
-1.5
-2.0
-2.5
-3.0
-3.5
-4.0
-4.5
-5.0
1.2
1.4
1.6
1.8
2.0

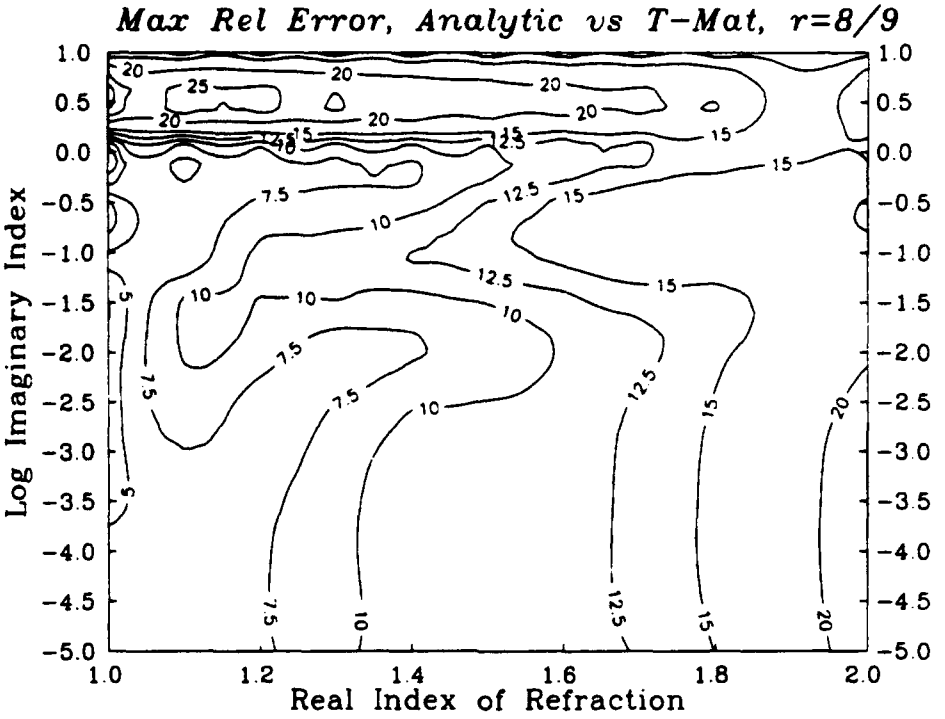
Max Rel Error, Analytic vs T-Mat, r=8/9
Log Imaginary Index
Real Index of Refraction
1.0
0.5
0.0
-0.5
-1.0
-1.5
-2.0
-2.5
-3.0
-3.5
-4.0
-4.5
-5.0
1.0
1.2
1.4
1.6
1.8
2.0

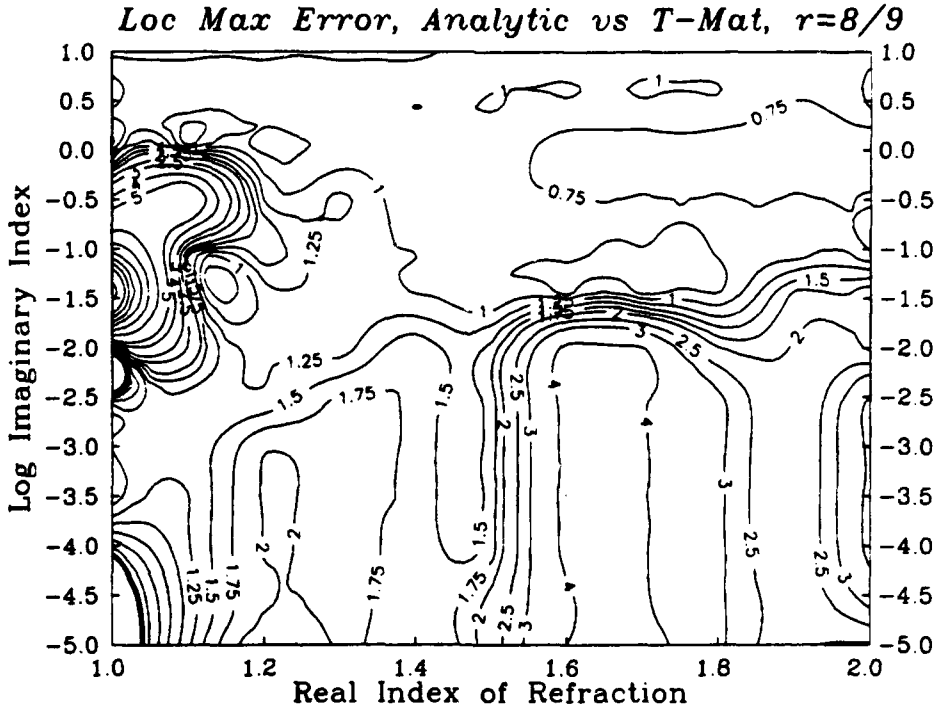
Loc Max Error, Analytic vs T-Mat, r=8/9
Log Imaginary Index
Real Index of Refraction
1.0
0.5
0.0
-0.5
-1.0
-1.5
-2.0
-2.5
-3.0
-3.5
-4.0
-4.5
-5.0
1.0
1.2
1.4
1.6
1.8
2.0

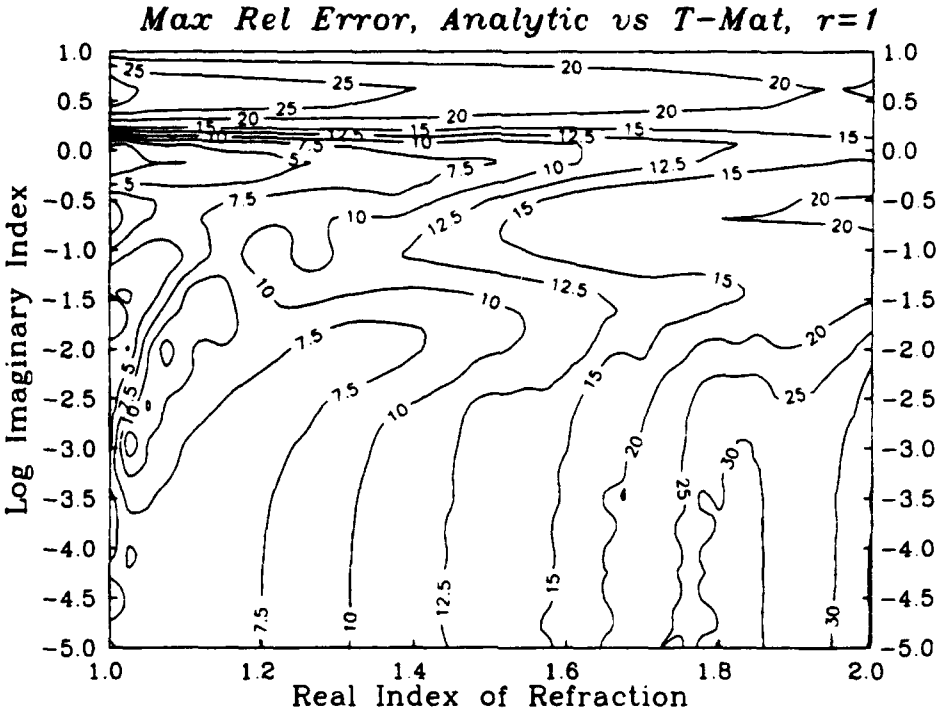
Max Rel Error, Analytic vs T-Mat, r=1
Log Imaginary Index
Real Index of Refraction
1.0
0.5
0.0
-0.5
-1.0
-1.5
-2.0
-2.5
-3.0
-3.5
-4.0
-4.5
-5.0
1.0
1.2
1.4
1.6
1.8
2.0

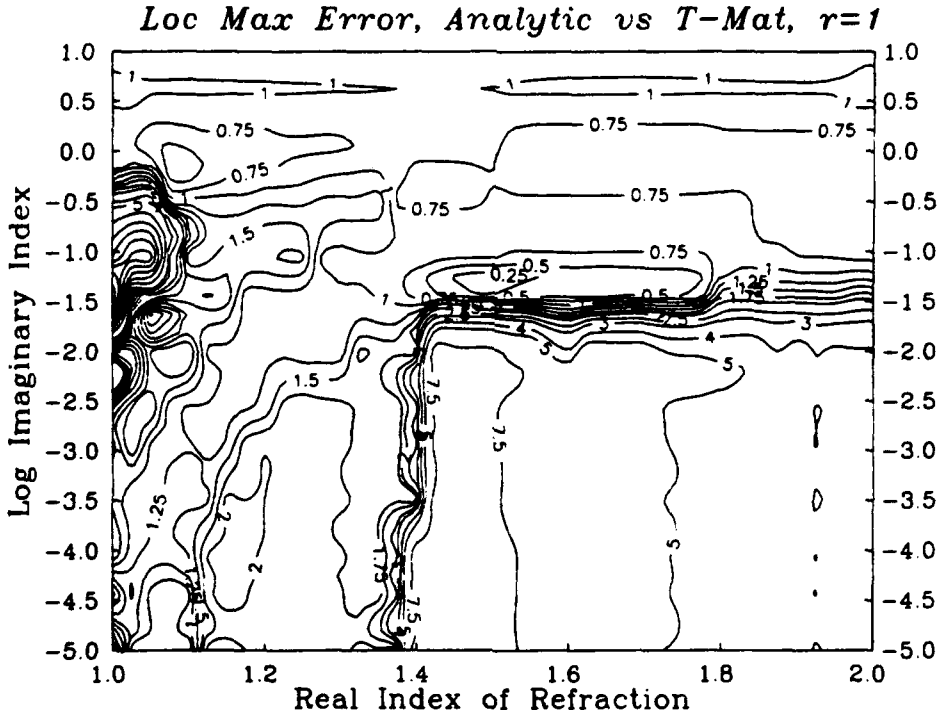
Loc Max Error, Analytic vs T-Mat, r=1
Log Imaginary Index
Real Index of Refraction
1.0
0.5
0.0
-0.5
-1.0
-1.5
-2.0
-2.5
-3.0
-3.5
-4.0
-4.5
-5.0
1.0
1.2
1.4
1.6
1.8
2.0

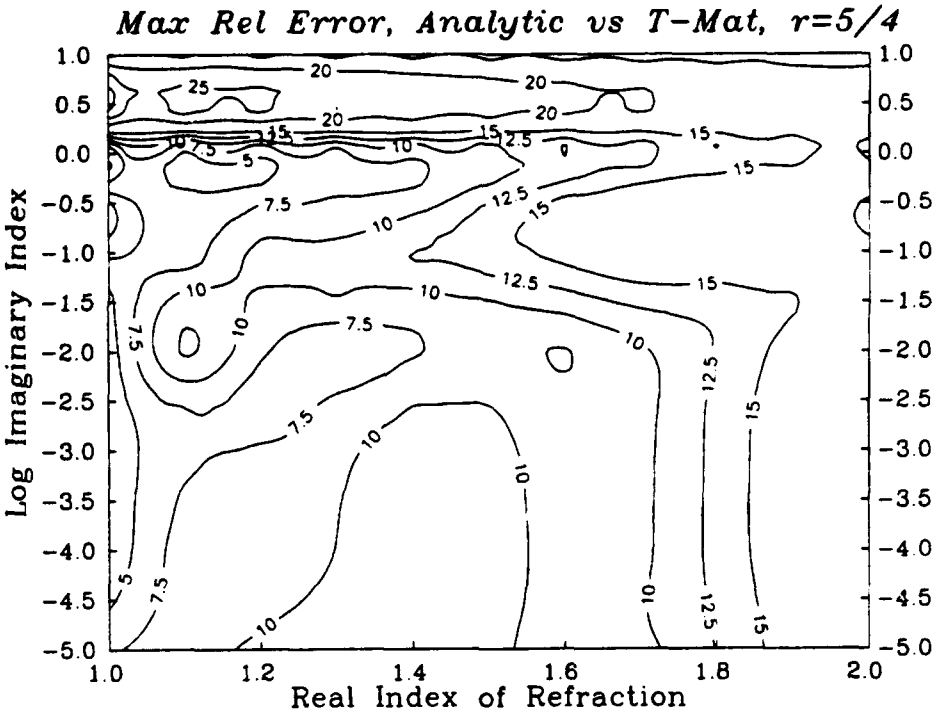
Max Rel Error, Analytic vs T-Mat, r=5/4
Log Imaginary Index
Real Index of Refraction
1.0
0.5
0.0
-0.5
-1.0
-1.5
-2.0
-2.5
-3.0
-3.5
-4.0
-4.5
-5.0
1.2
1.4
1.6
1.8
2.0

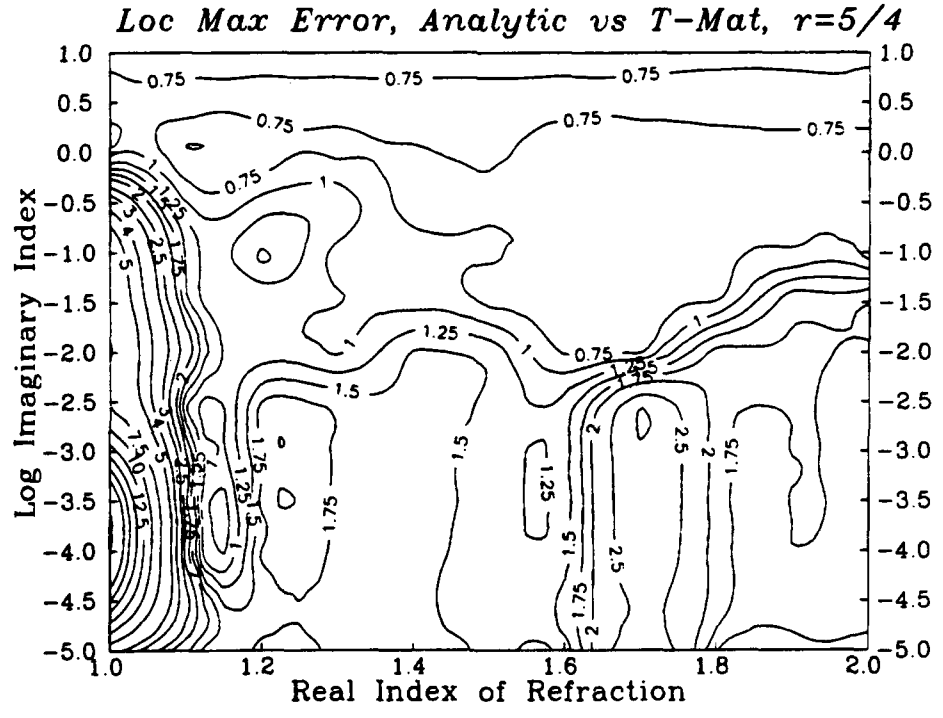
Loc Max Error, Analytic vs T-Mat, r=5/4
Log Imaginary Index
Real Index of Refraction
1.0
0.5
0.0
-0.5
-1.0
-1.5
-2.0
-2.5
-3.0
-3.5
-4.0
-4.5
-5.0
1.2
1.4
1.6
1.8
2.0

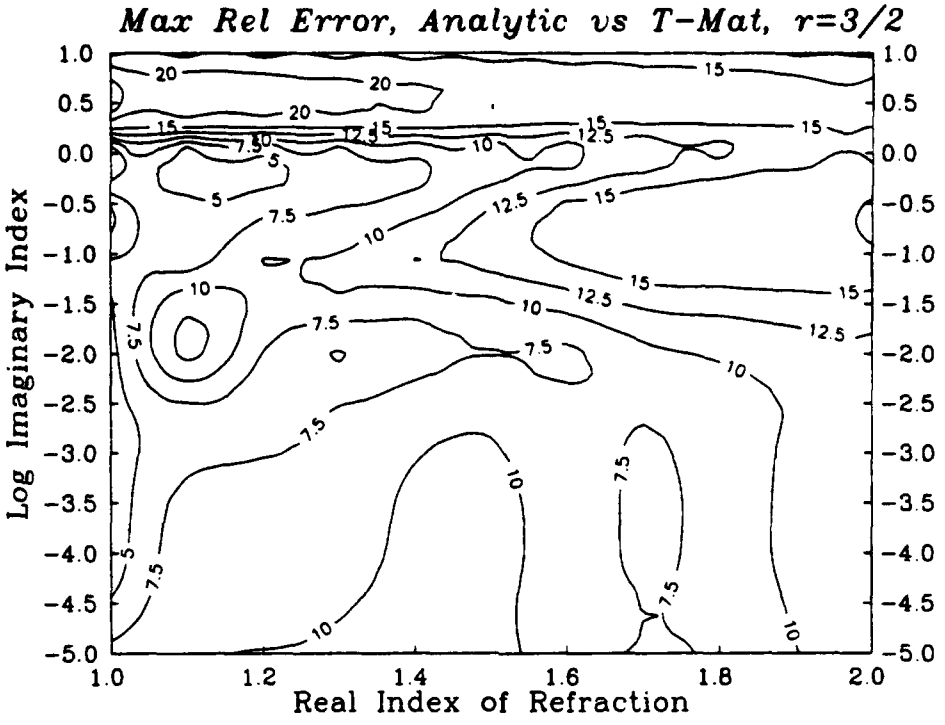
Max Rel Error, Analytic vs T-Mat, r=3/2
Log Imaginary Index
Real Index of Refraction
1.0
0.5
0.0
-0.5
-1.0
-1.5
-2.0
-2.5
-3.0
-3.5
-4.0
-4.5
-5.0
1.2
1.4
1.6
1.8
2.0

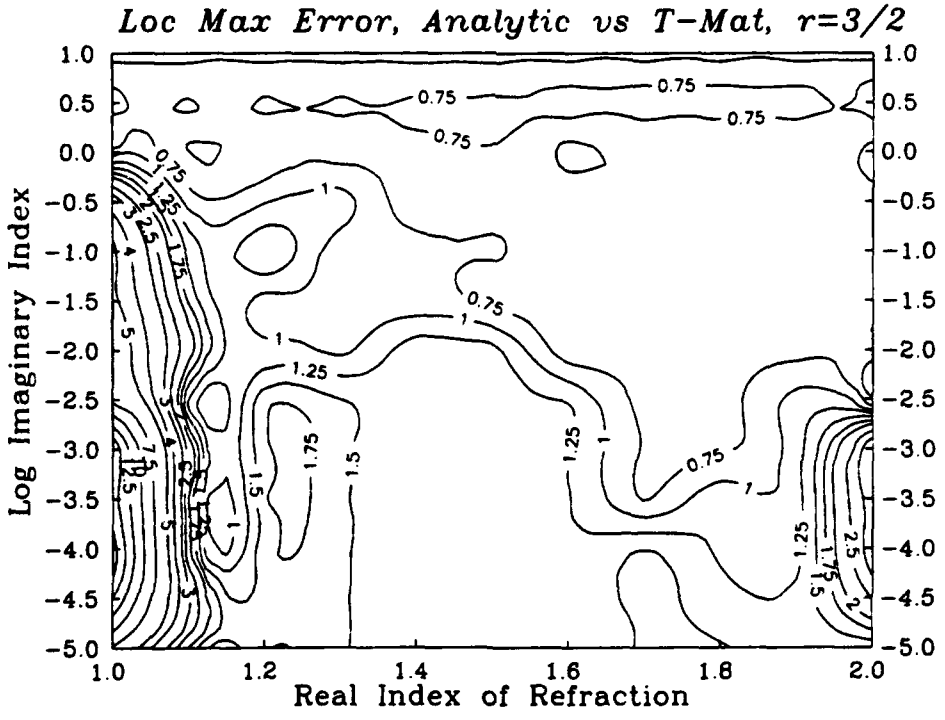
Loc Max Error, Analytic vs T-Mat, r=3/2
Log Imaginary Index
Real Index of Refraction
1.0
0.5
0.0
-0.5
-1.0
-1.5
-2.0
-2.5
-3.0
-3.5
-4.0
-4.5
-5.0
1.2
1.4
1.6
1.8
2.0

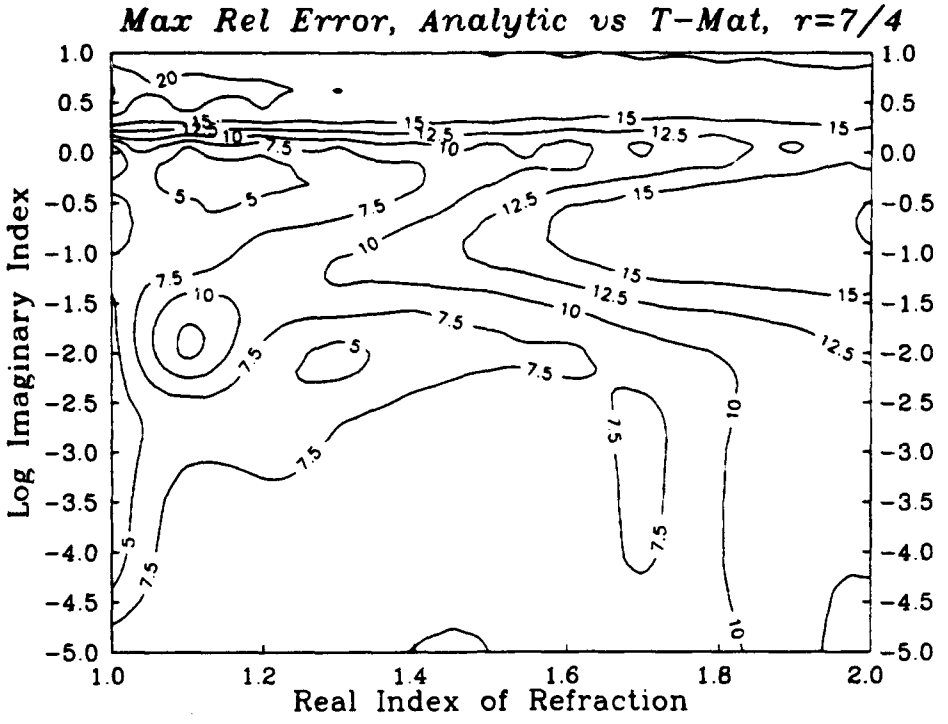
Max Rel Error, Analytic vs T-Mat, r=7/4
Log Imaginary Index
Real Index of Refraction
1.0
0.5
0.0
-0.5
-1.0
-1.5
-2.0
-2.5
-3.0
-3.5
-4.0
-4.5
-5.0
1.0
1.2
1.4
1.6
1.8
2.0
20
15
12.5
10
7.5
5

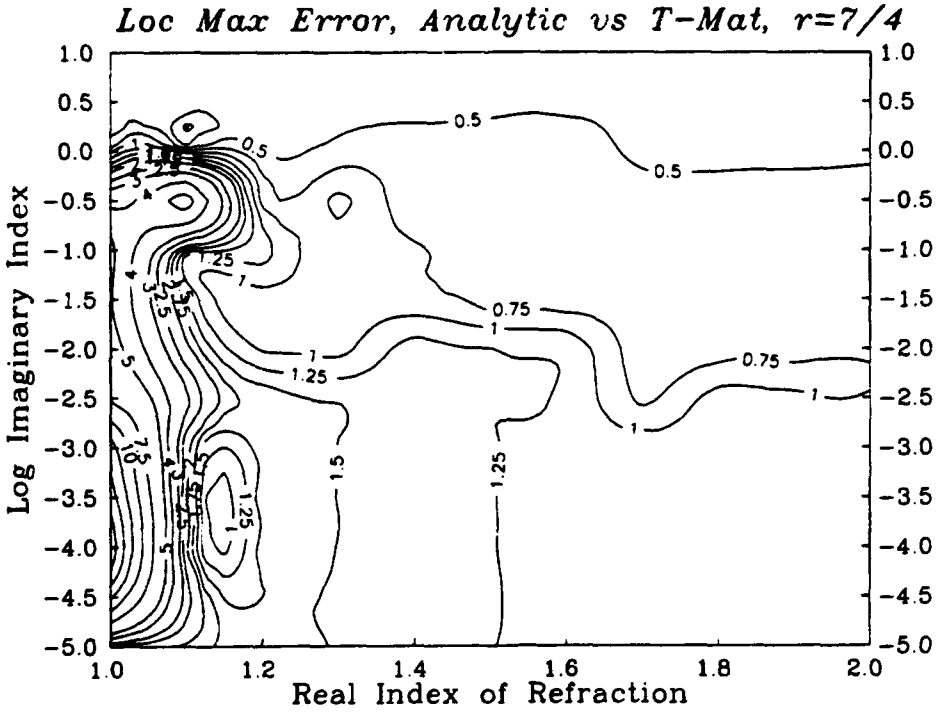
Loc Max Error, Analytic vs T-Mat, r=7/4
Log Imaginary Index
Real Index of Refraction
1.0
0.5
0.0
-0.5
-1.0
-1.5
-2.0
-2.5
-3.0
-3.5
-4.0
-4.5
-5.0
1.0
1.2
1.4
1.6
1.8
2.0
0.5
0.75
1
1.25
1.5

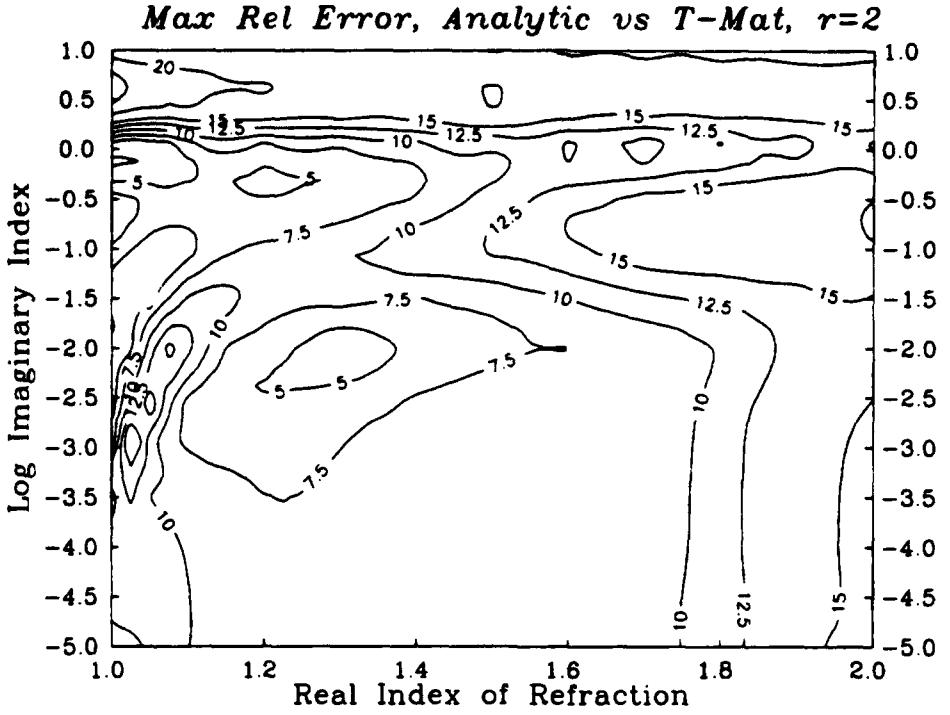
Max Rel Error, Analytic vs T-Mat, r=2
Log Imaginary Index
Real Index of Refraction
1.0
0.5
0.0
-0.5
-1.0
-1.5
-2.0
-2.5
-3.0
-3.5
-4.0
-4.5
-5.0
1.2
1.4
1.6
1.8
2.0

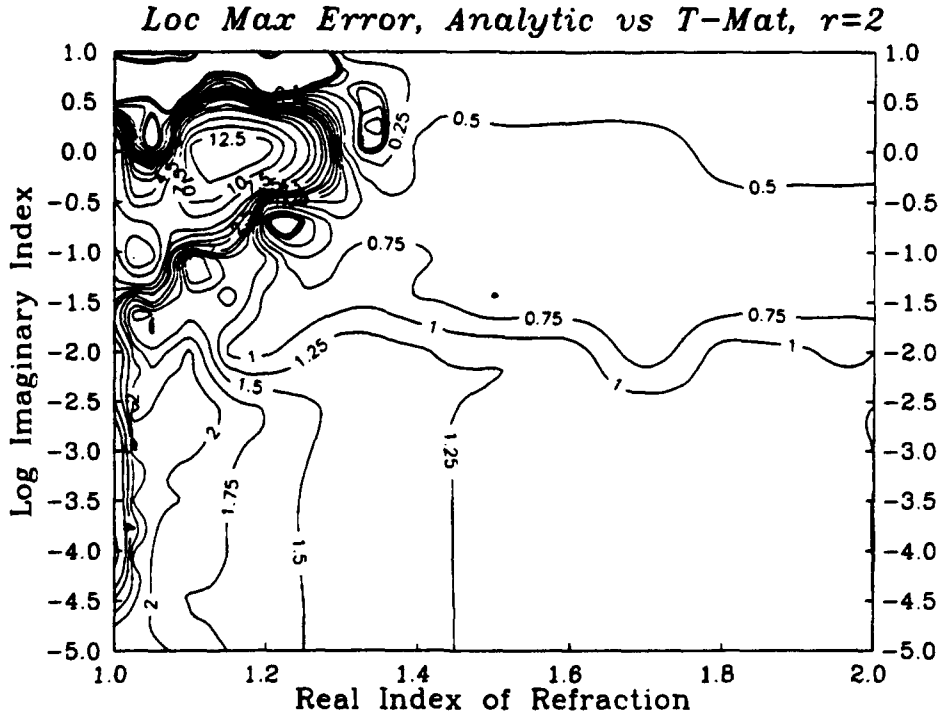
Loc Max Error, Analytic vs T-Mat, r=2
Log Imaginary Index
Real Index of Refraction
1.0
0.5
0.0
-0.5
-1.0
-1.5
-2.0
-2.5
-3.0
-3.5
-4.0
-4.5
-5.0
1.2
1.4
1.6
1.8
2.0

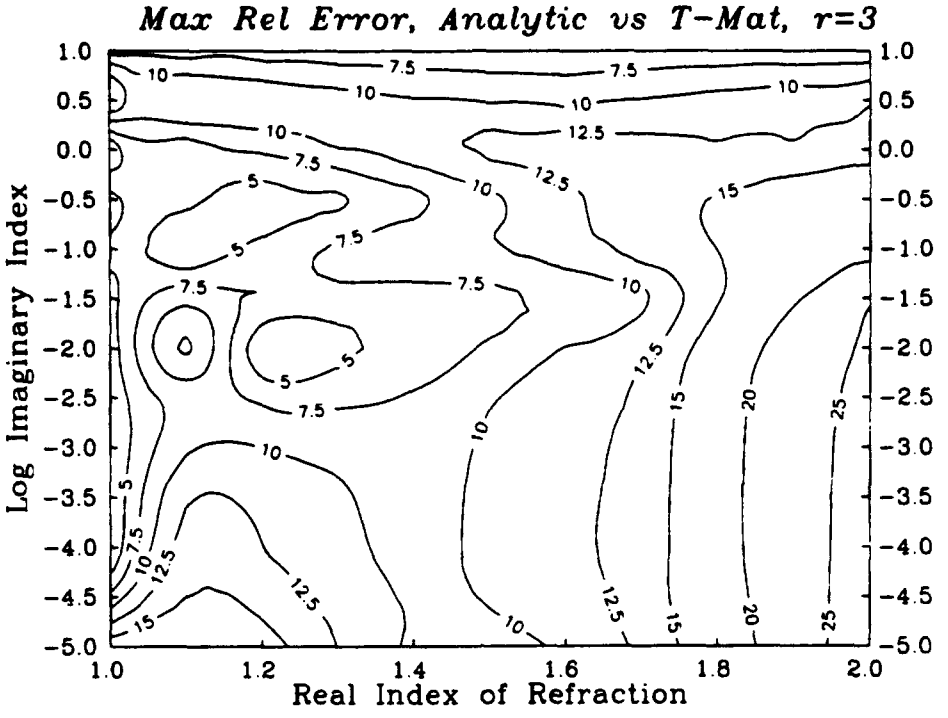
Max Rel Error, Analytic vs T-Mat, r=3
Log Imaginary Index
Real Index of Refraction
1.0
0.5
0.0
-0.5
-1.0
-1.5
-2.0
-2.5
-3.0
-3.5
-4.0
-4.5
-5.0
1.2
1.4
1.6
1.8
2.0

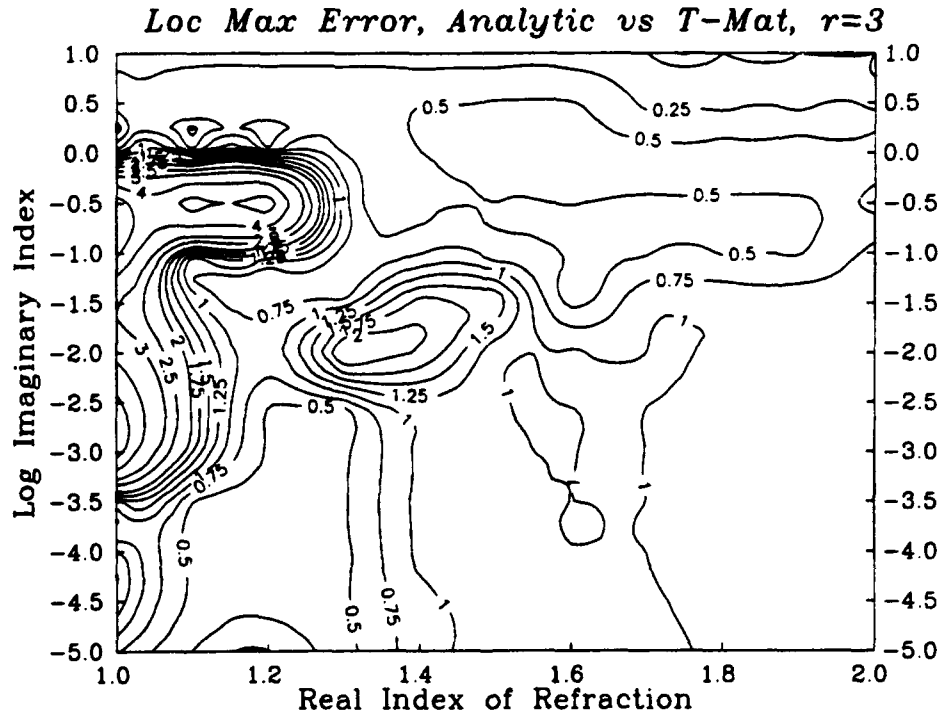
Loc Max Error, Analytic vs T-Mat, r=3
Log Imaginary Index
Real Index of Refraction
1.0
0.5
0.0
-0.5
-1.0
-1.5
-2.0
-2.5
-3.0
-3.5
-4.0
-4.5
-5.0
1.2
1.4
1.6
1.8
2.0

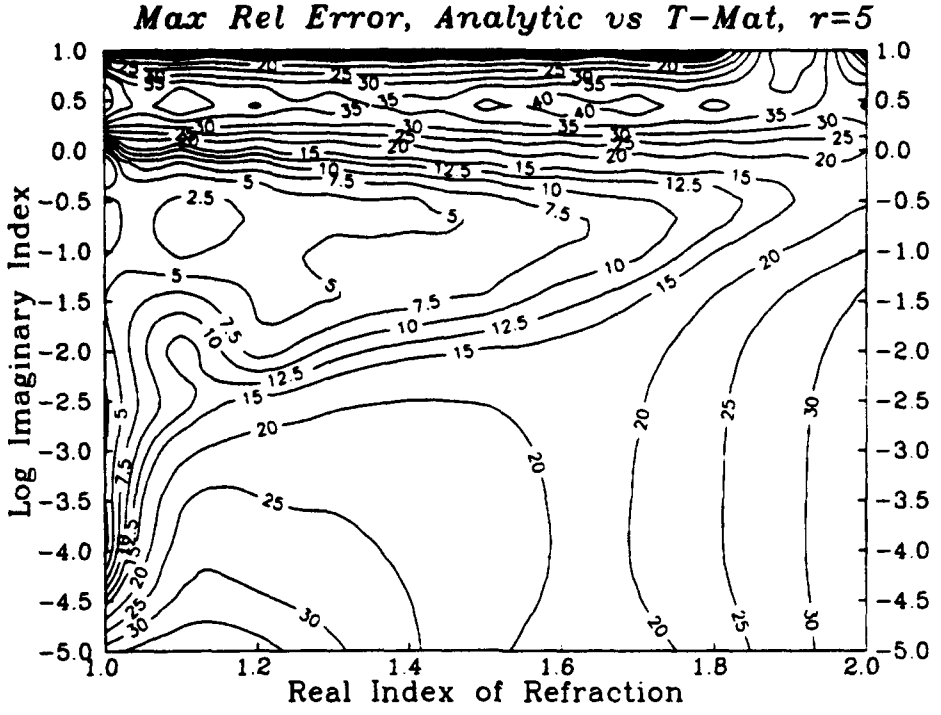
Max Rel Error, Analytic vs T-Mat, r=5
Log Imaginary Index
Real Index of Refraction
1.0
0.5
0.0
-0.5
-1.0
-1.5
-2.0
-2.5
-3.0
-3.5
-4.0
-4.5
-5.0
1.2
1.4
1.6
1.8
2.0

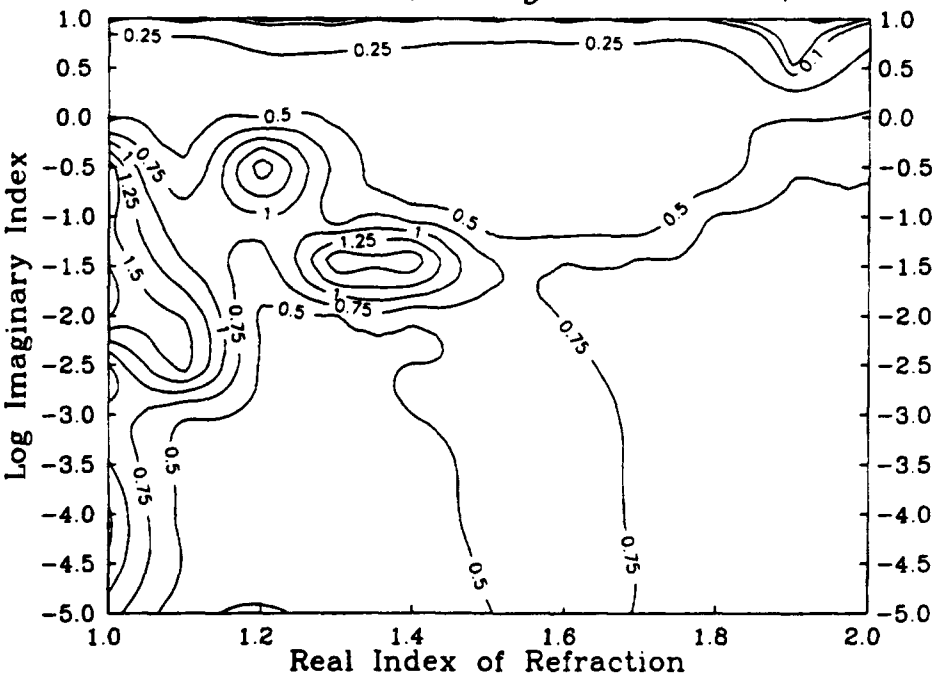
Loc Max Error, Analytic vs T-Mat, r=5
Log Imaginary Index
Real Index of Refraction
1.0
0.5
0.0
-0.5
-1.0
-1.5
-2.0
-2.5
-3.0
-3.5
-4.0
-4.5
-5.0
1.2
1.4
1.6
1.8
2.0

INTERNAL DISTRIBUTION

DREV R-4712/93

1 - Deputy Chief
1 - Director Electro-optics Division
1 - Director Energetic Materials Division
6 - Document Library
1 - Dr. B.T.N. Evans (author)
1 - Dr. G.R. Fournier (author)
1 - Dr. P. Pace
1 - Dr. L. Bissonnette
1 - Mr. D. Hutt
1 - Dr. G. Otis
1 - Mr. R. Kluchert
1 - Mr. G. Roy (Energetic Materials)
1 - Mr. G. Couture

EXTERNAL DISTRIBUTION

DREV R-4712/93

2 - DSIS
1 - CRAD
1 - DRDL
1 - DRDM
1 - DMCS
1 - National Library of Canada
1 - Micromedia Limited
1 - NRC/CISTI
1 - DRIC, U.K.
1 - DTIC, U.S.
1 - DISSLB, Australia

1 - Dr. W.G. Tam
Senior Project Manager
Industrial Research Assistance Program
Laboratory Network
National Research Council
Ottawa, Ontario
K1A 0R6

1 - Dr. A.I. Carswell
Dept. of Physics
York University
4700 Keele Street
North York, Ontario
M3J 1P3

1 - Dr. T. Platt
Biological Oceanography Division
Department of Fisheries and Oceans
Bedford Institute of Oceanography
P.O. Box 1006
Dartmouth, N.S. B2Y 4A2

1 - Dr. D. K. Cohoon
West Chester University
Dept. of Mathematics and Computer Science
West Chester, PA, 19383
USA

EXTERNAL DISTRIBUTION (contd)

DREV R-4712/93

1 – Dr. B.P. Curry
NPB Test Stand
Engineering Physics
Argonne National Lab.
9700 South Cass Ave., EP/207
Argonne, IL, 60439-4841
USA

1 – Dr. J. Embury
Chemical Research, Development and Engineering Center
SMCRR-RSP-B
Aberdeen Proving Ground, MD, 21010-5423
USA

1 – Dr. P. Barber
Clarkson College of Technology
Dept. of Electrical & Computer Engineering
Potsdam, NY, 13676
USA

1 – Dr. M. Lax
City College of New York
Physics Dept.
New York, NY, 10031
USA

1 – Dr. R.T. Wang
ISST- Space Astronomy Lab.
1810 NW 6th st.
Gainesville, FL, 32609
USA

1 – Dr. G. Kunz
Physics Laboratory TNO
P.O. Box 9 68 64
2509 The Hague
The Netherlands

EXTERNAL DISTRIBUTION (contd)

DREV R-4712/93

1 - Dr. C.M.P. Platt
CSIRO
Division of Atmospheric Research
Private Bag No. 1, Mordialloc, Vic 3195
Australia